

Tuning the strength of emergent correlations in a Brownian gas via batch resetting

Gabriele de Mauro,¹ Satya N. Majumdar,¹ and Grégory Schehr²

¹*LPTMS, CNRS, Université Paris-Saclay, 91405 Orsay, France*

²*Sorbonne Université, Laboratoire de Physique Théorique et Hautes Energies, CNRS UMR 7589, 4 Place Jussieu, 75252 Paris Cedex 05, France*

We study a gas of N diffusing particles on the line subject to *batch resetting*: at rate r , a uniformly random subset of m particles is reset to the origin. Despite the absence of interactions, the dynamics generates a nonequilibrium stationary state (NESS) with long-range correlations. We obtain exact results, both for the NESS and for the time dependence of the correlations, which are valid for arbitrary m and N . By varying m , the system interpolates between an uncorrelated regime ($m = 1$) and the fully synchronous resetting case ($m = N$). For all $1 < m < N$, correlations exhibit a non-monotonic time dependence due to the emergence of an intrinsic decorrelation mechanism. In the stationary state, the correlation strength can be tuned by varying m , and it displays a transition at a critical value $N_c = 6$. Our predictions extend straightforwardly to any spatial dimension d and the critical value $N_c = 6$ remains the same in all dimensions. Our predictions are testable in existing experimental setups on optically trapped colloidal particles.

Stochastic resetting was introduced in [1, 2] with the simple idea: the dynamics of a system is interrupted at random times and restarted from a fixed initial condition. This mechanism is very general and it can be applied to any deterministic or stochastic dynamics. It has attracted substantial theoretical and experimental interest because of its nontrivial effects on the behavior of various systems. For example, by breaking detailed balance, the stochastic resetting drives the system to a nonequilibrium stationary state (NESS) [1–9]. Also, stochastic resetting can dramatically enhance the efficiency of search processes [1–4, 10–32]. More recently, striking dynamical effects have been uncovered in systems where many degrees of freedom (DOF) are all reset simultaneously. In particular, a one-dimensional gas of N independent Brownian particles, all reset simultaneously to the origin at a rate r , develops strong long-range correlations and reaches a NESS that, though strongly correlated, remains analytically tractable for physically measurable observables [33]. These correlations arise purely from the dynamics: although the particles never interact, the *simultaneity* of the resets couples all DOF and induces effective correlations. Such dynamically emergent correlations (DEC) have been observed in several systems in which the DOF do not interact directly, but they get strongly correlated by a shared fluctuating environment [32–44].

In the examples mentioned above, all DOF are coupled to the same single fluctuating environment that acts globally. This naturally raises the question of what survives of this phenomenology when environmental fluctuations act only on a subset of the DOF at the same time. We show below that this change induces a qualitatively different physics in the system and its analytical treatment becomes highly nontrivial. Previous works have considered partitioned systems, in which the DOF are split into two subsets: one is repeatedly reset, whereas the other is never reset. It was shown in [45, 46] that one can control the stationary state of the full system by a repeated

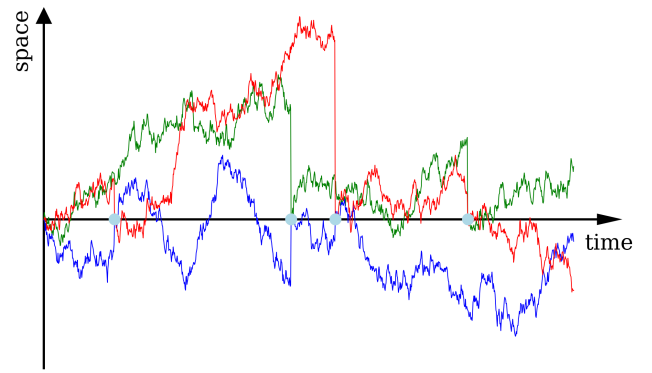


FIG. 1: Schematic representation of batch resetting for $N = 3$ and $m = 2$. Four resetting events are shown (light-blue dots).

resetting of only one of the subsystems. However, this requires the two subsystems to have an extensive number of long-range interactions. What we study here is fundamentally different: in our system, direct interactions between the DOF are completely absent. In addition, all DOF are coupled to the same fluctuating environment, but each fluctuation acts only on a randomly chosen subset rather than on the whole system. Over long times, these repeated fluctuations ensure that every DOF is intermittently affected.

Concretely, we introduce *batch resetting*, the simplest, yet already very interesting, setting to study this phenomenon. We consider a one-dimensional system of N diffusing particles (with diffusion constant D) that undergo stochastic resetting at a constant rate r . At each reset event, only m particles, chosen uniformly at random, are reset to the origin, while the remaining $N - m$ particles keep diffusing (see Fig. 1). Thus, the fluctuating environment is effectively generated by the stochastic resetting of a randomly selected subset of m particles,

where the subset is independently re-sampled at every event. It is important to stress that the problem becomes mathematically far more difficult as soon as $m \neq N$. When all N particles are reset together ($m = N$), the dynamics obey a simple renewal equation that directly yields the stationary state [3, 33]. For any intermediate value $1 \leq m < N$, however, this renewal structure is lost: since only a subset of DOF is reset, the system never returns to a fully renewed configuration. As a result, the renewal equation breaks down and the standard methods used for simultaneous resetting no longer apply. In this Letter, we develop an alternative approach, based on the Fokker–Planck equation, that allows us to tackle this substantially more challenging case.

Our analysis shows that batch resetting generates robust long-range attractive correlations even for $m < N$. We show that the correlation strength can be tuned through the single parameter m , interpolating between an uncorrelated stationary state at $m = 1$ and the fully synchronous limit at $m = N$. Moreover, new phenomena appear for $m < N$. First, the system develops non-monotonic correlations in time due to a new decorrelation mechanism with a characteristic timescale that diverges as $m \rightarrow N$. Its origin is discussed below. Second, these strong, attractive correlations persist all the way to the NESS, where we uncover a transition in the shape of the stationary correlations as a function of m when the total number of particles N crosses a critical value $N_c = 6$.

Recent experiments have made stochastic resetting directly accessible in the lab. Colloidal particles diffusing in water can now be reset using laser-generated optical traps, both individually [47–50] and in groups [51, 52]. Notably, in Ref. [52], each particle is confined in its individual optical trap, and the stiffnesses of all the traps are synchronously modulated at random times, effectively implementing simultaneous resetting events. This setup offers a direct route to test our predictions for batch resetting, as each particle being in its own trap allows selective resetting of any subset of m particles.

To study the case $m < N$ we develop a Fokker–Planck approach. We denote by $P_m(\mathbf{x}, t)$ the joint probability density function (JPDF) of the system, where $\mathbf{x} = \{x_1, \dots, x_N\}$ are the positions of the particles and the subscript m indicates that exactly m particles are reset at each event. It is convenient to introduce its Fourier transform (FT)

$$\tilde{P}_m(\mathbf{k}, t) = \int d\mathbf{x} e^{i\mathbf{k} \cdot \mathbf{x}} P_m(\mathbf{x}, t), \quad \mathbf{k} = (k_1, \dots, k_N), \quad (1)$$

which we refer to as the FT–JPDF. We also define the n -point marginals of the JPDF as $P_m^n(x_1, \dots, x_n, t) = \int dx_{n+1} \dots dx_N P_m(\mathbf{x}, t)$, with FT $\tilde{P}_m^n(k_1, \dots, k_n, t) = \int dx_1 \dots dx_n e^{i(k_1 x_1 + \dots + k_n x_n)} P_m^n(x_1, \dots, x_n, t)$. We recall that, in batch resetting protocol, at each resetting event, a subset $S_m \subseteq \{1, \dots, N\}$ of size $|S_m| = m$ is selected uniformly at random. For those particles whose labels belong

to S_m , the position is set to zero. The goal is to write a Fokker–Planck equation for this batch resetting protocol. This can be done either in the real space or in the Fourier space (which is slightly simpler). In the Supplemental Material (SM) [53], we derive the Fokker–Planck equation for both representations. Here, for convenience, we describe the form in Fourier space

$$\begin{aligned} \partial_t \tilde{P}_m(\mathbf{k}, t) &= -(Dk^2 + r) \tilde{P}_m(\mathbf{k}, t) \\ &+ \frac{r}{\binom{N}{m}} \sum_{S_m} \tilde{P}_m^{N-m}(\mathbf{k}_{S_m^c}, t), \end{aligned} \quad (2)$$

while the one in direct space is given in (10) of the End Matter. The first term in (2), $-Dk^2 \tilde{P}_m(\mathbf{k}, t)$, corresponds to standard diffusion, where $k^2 = |\mathbf{k}|^2 = \sum_{i=1}^N k_i^2$. The second contribution, $-r \tilde{P}_m(\mathbf{k}, t)$, represents the loss of probability induced by resetting events occurring at rate r . The last term encodes the gain of probability coming from all possible resetting events. Recalling that the positions of particles whose labels belong to S_m are set to zero, it follows that, in Fourier space, one needs to set the corresponding Fourier momentum $k_i = 0$, as explained in detail in the SM [53]. It is convenient to also define the set $S_m^c = \{1, \dots, N\} \setminus S_m$ and the vector $\mathbf{k}_{S_m^c}$, which is obtained from $\mathbf{k} = (k_1, \dots, k_N)$ by setting to zero the components $\{k_i\}_{i \in S_m}$. Accordingly, $\tilde{P}_m^{N-m}(\mathbf{k}_{S_m^c}, t)$ denotes the $(N-m)$ -point marginal in Fourier space, evaluated at $\mathbf{k}_{S_m^c}$. Averaging this contribution over all $\binom{N}{m}$ possible reset subsets of size m produces the factor $1/\binom{N}{m}$ in (2). The notations in (2) may look a bit abstract, but they become clearer by explicitly considering a simple example, such as $N = 3$ and $m = 2$ (this example is worked out in detail in the SM [53]).

The FP equation in (2) has an interesting structure, namely, that the equation for the m -th marginal of the FT–JPDF involves only marginals up to m on the right hand side and not higher order. Consequently, the full time-dependent solution of the m -th marginal $\tilde{P}_m(\mathbf{k}, t)$ can, in principle, be solved recursively. The stationary solution is easier as one needs to set the time derivative in (2) to zero. This leads to a closed set of equations characterizing the stationary FT–JPDF and all its marginals. In particular, it provides an exact solution for the JPDF when $m = N-1$ and $m = 1$ (see SM [53]), in addition to the known result for $m = N$. For a general $1 < m < N-1$, an exact solution remains possible in principle but cumbersome to find in practice. Nevertheless, the one- and two-point marginals can still be obtained in compact closed form for all m

$$\tilde{P}_m^1(k) = \frac{1}{1 + \ell_m^2 k^2}, \quad \text{where} \quad \ell_m^2 = \frac{D}{\tilde{r}}, \quad \tilde{r} = \frac{m}{N} r, \quad (3)$$

and

$$\tilde{P}_m^2(k_1, k_2) = \frac{(2-\beta) + (\beta-1) [\tilde{P}_m^1(k_1) + \tilde{P}_m^1(k_2)]}{\beta + \ell_m^2 (k_1^2 + k_2^2)}. \quad (4)$$

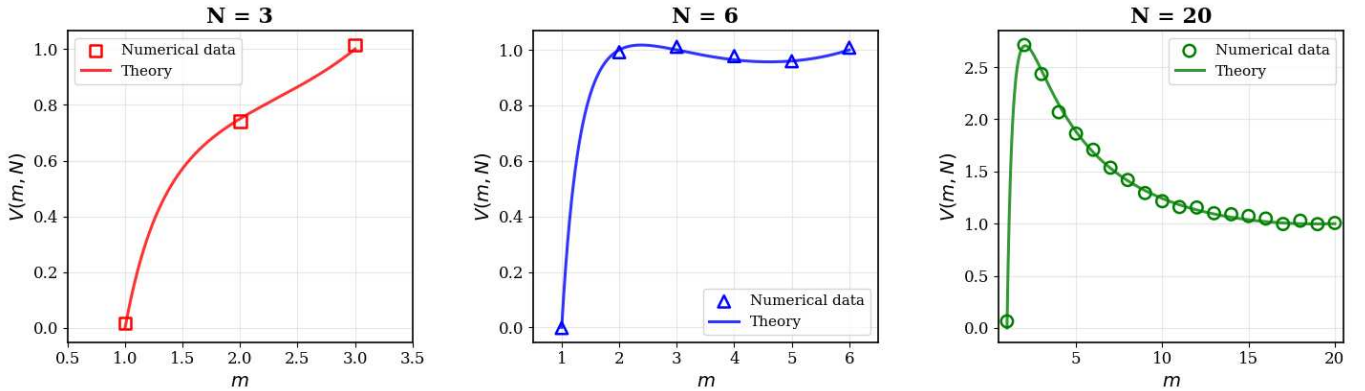


FIG. 2: Plot of the function $V(m, N)$ (Eq. (8)) compared with numerical simulations, shown as a function of m for different values of N . For $N < N_c = 6$, $V(m, N)$ increases monotonically with m , whereas for $N > N_c$ it becomes non-monotonic: the global maximum shifts from $m = N$ to $m = 2$ and a shallow local minimum develops at $m = N - 1$. This minimum is clearly visible in the central panel but it is also present for all $N \geq N_c$. At the critical value $N = N_c$, the points $m = 2, 3, N$ all give the same maximal value $V(m, N_c) = 1$. The rightmost point corresponds to fully synchronous resetting [33] for all values of N .

The parameter $\beta = \frac{2N-m-1}{N-1} \in [1, 2]$ interpolates between $\beta = 1$ as $m \rightarrow N$ and $\beta = 2$ as $m \rightarrow 1$. By inverting the FTs in (3) and (4) we obtain

$$P_m^1(x) = \frac{1}{\ell_m} \mathcal{R}\left(\frac{x}{\ell_m}\right), \quad \mathcal{R}(u) = \frac{1}{2} e^{-|u|}, \quad (5)$$

while $P_m^2(x_1, x_2)$, which can be expressed explicitly in terms of integrals involving Bessel functions, is given in Eq. (15) in the End Matter.

Since all particles are statistically equivalent in our system, the average density of particles $\rho_N^m(x) = \frac{1}{N} \langle \sum_{i=1}^N \delta(x - x_i) \rangle$ coincides with the one-point marginal $P_m^1(x)$ given above, namely $\rho_N^m(x) = P_m^1(x) = \frac{1}{\ell_m} \mathcal{R}(x/\ell_m)$. This function decays exponentially over the length scale $\ell_m = \sqrt{\frac{ND}{mr}} \sim O(1/\sqrt{m/N})$, which decreases as the fraction of reset particles increases. However, the scaling function $\mathcal{R}(u)$ is independent of both m and N , and is therefore identical to the fully synchronous case [33]. In this sense, all one-particle observables are insensitive to whether resets involve all particles or only a subset, up to the simple rescaling $r \rightarrow \tilde{r} = \frac{m}{N}r$. In contrast, the two-point marginal $P_m^2(x_1, x_2)$ acquires a qualitatively different structure for $m < N$ (see SM [53]), leading to new phenomena in the two-particle observables, such as the emergence of nontrivial two-point correlations, as discussed below.

To quantify the DEC between two particles, it is natural to consider the standard two-point correlation function $\langle x_i(t)x_j(t) \rangle - \langle x_i(t) \rangle \langle x_j(t) \rangle$. However, due to the $x_i \rightarrow -x_i$ symmetry in this system, this standard correlator is identically zero. Hence, to detect the correlations, the simplest and the natural quantity is the next-order correlator

$$C_{ij} = \langle x_i^2(t)x_j^2(t) \rangle - \langle x_i^2(t) \rangle \langle x_j^2(t) \rangle, \quad i, j \in \{1, 2\}, \quad (6)$$

where $\langle \cdot \rangle$ denotes the average with respect to the JPDF $P_m(\mathbf{x}, t)$. Using the permutation symmetry, it follows that $C_{ii} = \mathcal{C}_1(t) \forall i$, and $C_{ij} = \mathcal{C}_2(t) \forall i \neq j$. Note that $\mathcal{C}_2(t)$ encodes both correlations and fluctuations, while $\mathcal{C}_1(t)$ contains only information about fluctuations. Hence, to isolate only the correlation part, it is natural to consider the normalised correlator

$$a(t; m, N) = \frac{\mathcal{C}_2(t)}{\mathcal{C}_1(t)} = \frac{\langle x_i^2(t)x_j^2(t) \rangle - \langle x_i^2(t) \rangle \langle x_j^2(t) \rangle}{\langle x_i^4(t) \rangle - \langle x_i^2(t) \rangle^2}. \quad (7)$$

One can show that $0 \leq a(t; m, N) \leq 1$, interpolating between the completely uncorrelated case and the fully correlated case where $x_i^2 = x_j^2 \forall (i, j)$. These quantities were studied previously for the fully synchronous resetting $m = N$ [33, 41, 42]. We show that these functions can also be computed exactly for the batch resetting protocol, for any $1 \leq m \leq N$, thus enabling a direct comparison with the fully synchronous case. The complete derivations are provided in the End Matter in Eqs. (18)-(20). Here we just summarise the main results.

We first consider $\mathcal{C}_2(t)$ and in particular its stationary limit $\mathcal{C}_2^* = \mathcal{C}_2(t \rightarrow \infty)$. We find that it can be expressed as (see End Matter)

$$\mathcal{C}_2^* = \frac{4D^2}{r^2} V(m, N), \quad V(m, N) = \frac{N^2(m-1)}{m^2(2N-m-1)}. \quad (8)$$

In the fully synchronous case ($m = N$) one recovers the known results $\mathcal{C}_2^* = \frac{4D^2}{r^2}$ [33]. The function $V(m, N)$, shown in Fig. 2, satisfies $V(N, N) = 1$ and $V(1, N) = 0$ for all N , and it is strictly positive for any $N > 1$ and $1 < m < N$. This shows that the attractive correlations characteristic of fully synchronous resetting persist for all $1 < m < N$. Moreover, varying m provides a simple way to tune the strength of the correlations. In addition, we uncover an intriguing transition in the behavior of

the stationary correlations as a function of m when the total number of particles crosses $N_c = 6$. As seen in Fig. 2, for $N < N_c$ the correlation strength increases monotonically with m , while for $N > N_c$ it becomes non-monotonic and the global maximum shifts from $m = N$ to $m = 2$. For $N \geq N_c$, the function also develops a shallow local minimum at $m = N - 1$, before increasing again to the fully synchronous value $V(N, N) = 1$, as illustrated in the central panel of Fig. 2. At $N = N_c$ the maximum is not unique, since at $m = 2, 3, 6$ the function $V(m, N_c)$ attains the same maximal value 1. This nontrivial dependence on m arises from the competition between two effects to which the correlator C_2^* is sensitive: single-particle fluctuations and two-particle correlations. In particular, increasing m makes each reset event involve more particles, so correlations are injected into a larger group at once. However, a larger value of m also means that each particle is reset more frequently and therefore explores a smaller region between two of its own resets, of size $\ell_m \sim O(1/\sqrt{m/N})$. Thus, as m increases, these two trends compete: the contribution to C_2^* coming from correlations grows, since more particles are simultaneously reset, while the contribution coming from single-particle fluctuations decreases, as the explored region ℓ_m becomes smaller. Their interplay gives rise to the observed non-monotonic behavior when $N \geq 6$. This becomes clearer if we normalize the correlations by the typical fluctuations of a single particle, which are captured by the object $C_1(t)$. This removes the dependence on the exploration range ℓ_m and isolates the sole effect of resetting larger groups. In these units, the stationary correlator takes the form $a(t \rightarrow \infty; m, N) = \frac{C_2(t \rightarrow \infty)}{C_1(t \rightarrow \infty)} = \frac{1}{5} \frac{m-1}{2N-m-1}$, which is strictly monotonic in m for any fixed N .

The second key result of this Letter concerns the time dependence of the function $a(t; m, N)$. It takes the scaling form $a(z = \tilde{r}t; m, N) \equiv A(z; \beta)$, where $A(z; \beta)$ depends on m and N only through $\beta = (2N - m - 1)/(N - 1)$, and its explicit form is reported in Eq. (20) of the End Matter. Indeed, one can write a closed evolution equation for $A(z; \beta)$ as a function of the rescaled time $z = \tilde{r}t$ and identify different loss and gain terms due to the batch resetting protocol. This is done in detail in Section S7 of the SM [53]. By solving this equation for $A(z; \beta)$ for all z , we obtain the results shown in Fig. 3. As expected, for $m = 1$ ($\beta = 2$) the function vanishes identically since the particles never interact. In contrast, for $m = N$ ($\beta = 1$) it increases monotonically with z (see Fig. 3). A key finding of this work is that this behavior changes qualitatively as soon as $m < N$. For any $1 < m < N$ ($1 < \beta < 2$), the function $A(z; \beta)$ becomes non-monotonic: it first grows (correlation-building phase), then decreases (decorrelation phase), and finally saturates to the stationary value $A(z \rightarrow \infty; \beta) = \frac{1}{5} \left(\frac{2}{\beta} - 1 \right)$ (see Fig. 3), developing a maximum at a finite time $z = z^*(\beta)$.

This non-monotonicity originates from a decorrelating

mechanism which is absent for $m = N$ (see Section S7 of SM [53]). It can be understood as follows. Consider two fixed particles: when $m < N$, one may reset while the other does not, erasing their pre-existing correlations. This introduces an additional timescale into the dynamics, which is responsible for the appearance of the finite-time maximum, and it diverges as $\beta \rightarrow 1^+$. Although a closed expression for the position $z^*(\beta)$ of the maximum is hard to find for general β , analytic progress can be made in the limits $\beta \rightarrow 1^+$ and $\beta \rightarrow 2^-$. For the first case, it is

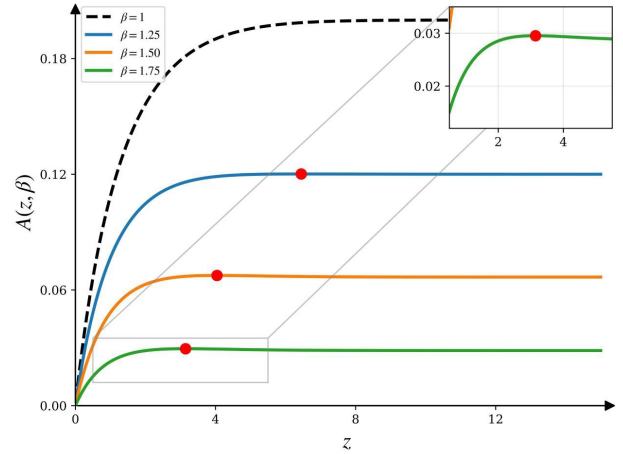


FIG. 3: Scaling function $A(z; \beta)$ defined in Eq. (20) of the End Matter, shown for several values of $\beta = \frac{2N-m-1}{N-1} \in [1, 2]$. For $1 < m < N$ ($1 < \beta < 2$), $A(z; \beta)$ develops a maximum at a finite time z (indicated by red dots), while for $m = N$ ($\beta = 1$) it increases monotonically. For any $1 < \beta < 2$, $A(z; \beta)$ decays exponentially fast to its stationary value $(2/\beta - 1)/5$.

convenient to introduce the parameter $\epsilon = \frac{N-m}{N-1}$, so that $\beta = 1 + \epsilon$ and $\epsilon \rightarrow 0$ corresponds to the fully synchronous limit $m \rightarrow N$. Here we consider N to be large, so that ϵ may be treated as a continuous small parameter. In this regime (see SM [53]), we obtain the asymptotic expansion

$$z^*(\epsilon) = \frac{a_0}{\epsilon} + a_1 + O(\epsilon), \quad (9)$$

where $a_0 = 1.1262\dots$ is the root of the equation $e^{a_0}(5 - 3a_0) = 5$, and $a_1 = 2$. In the opposite limit $\beta \rightarrow 2^-$ (corresponding to $N \rightarrow \infty$ with $m > 1$), the amplitude of the scaling function $A(z; \beta)$ vanishes, as correlations disappear when particles are never reset together. However, as $\beta \rightarrow 2^-$ the position of the maximum freezes to $\bar{z} = 2.6495\dots$, where \bar{z} is the solution of a transcendental equation [see (22) in the End Matter]. Very recently, a similar non-monotonic behavior of $A(z; \beta)$ was found in a system where N diffusing particles are reset simultaneously to previously visited positions, thus introducing an explicit temporal memory kernel [42]. There, the non-monotonicity appears only below a certain threshold of the control parameter and was characterized mostly through numerical analysis. Our batch resetting protocol provides

a complementary example: non-monotonic temporal correlations arise for all $1 < m < N$ (i.e., $1 < \beta < 2$) without the need for an explicit memory kernel, and the position $z^*(\beta)$ of the maximum can be investigated analytically in the limits $\beta \rightarrow 1^+$ and $\beta \rightarrow 2^-$.

For finite N , the discussion above sheds light on the correlations between individual particles ensuing from the batch resetting protocol. It is natural to wonder what happens in the large N limit, where our system resembles a strongly correlated gas of particles on a line. For such a continuum many-body system, it is natural to coarse-grain the system and define a local empirical density $\hat{\rho}(x) = \frac{1}{N} \sum_{i=1}^N \delta(x - x_i)$. The natural way to probe the correlations in this continuum coarse-grained system is to study the density-density correlation function or its Fourier transform, known as the spectral form factor. We show in the SM [53] that these observables can be computed exactly in our system and they exhibit interesting new behaviours that can also be traced back to the batch resetting protocol.

To conclude, batch resetting generates strong and tunable long-range correlations in a diffusive gas. One-particle observables remain identical to the fully synchronous case, up to a rescaling of the resetting rate. In contrast, two-particle observables display qualitatively new behaviors, including non-monotonic temporal correlations and a transition in the stationary correlation strength at $N_c = 6$ as a function of m . Our exact solution provides a unified framework to interpret these effects and yields quantitative predictions. These predictions are directly testable in the optical-trap setup of Ref. [52], which can implement batch resetting, in principle, by modulating only m out of N traps (with up to $N = 8$).

Additionally, our analysis extends straightforwardly to higher spatial dimensions. In any spatial dimension d , the normalized correlation function in $A(z; \beta)$ remains non-monotonic in z , and, interestingly, the function $V(m, N)$ remains the same in all d , thus exhibiting the same transition at $N_c = 6$ (see SM [53] for a derivation). This further demonstrates the robustness of our results.

From a theoretical perspective, it would be natural to explore the case where the number of reset particles m is itself random, or to explore implications for search processes. In the fully synchronous case $m = N$, a transition occurs at a critical team size $N = \bar{N}_c$, separating regimes where resetting is beneficial or detrimental to search efficiency [22]. It would be interesting to investigate how this behavior is modified under batch resetting and whether asynchronous resetting can enhance multi-agent search strategies.

Acknowledgments. We acknowledge support from ANR Grant No. ANR-23-CE30-0020-01 EDIPS.

[1] M. R. Evans, S. N. Majumdar, Phys. Rev. Lett. **106**, 160601 (2011).

- [2] M. R. Evans, S. N. Majumdar, J. Phys. A: Math. Theor. **44**, 435001 (2011).
- [3] M. R. Evans, S. N. Majumdar, G. Schehr, J. Phys. A: Math. Theor. **53**, 193001 (2020).
- [4] A. Pal, S. Kostinski, S. Reuveni, J. Phys. A: Math. Theor. **55**, 021001 (2022).
- [5] S. Gupta, A. M. Jayannavar, Front. Phys. **10**, 789097 (2022).
- [6] A. Nagar, S. Gupta, J. Phys. A: Math. Theor. **56**, 283001 (2023).
- [7] S. Gupta, S. N. Majumdar, G. Schehr, Phys. Rev. Lett. **112**, 220601 (2014).
- [8] U. Basu, A. Kundu, A. Pal, Phys. Rev. E **100**, 032136 (2019).
- [9] M. Magoni, S. N. Majumdar, G. Schehr, Phys. Rev. Research **2**, 033182 (2020).
- [10] M. R. Evans, S. N. Majumdar, J. Phys. A: Math. Theor. **47**, 285001 (2014).
- [11] L. Kusmierz, S. N. Majumdar, S. Sabhapandit, G. Schehr, Phys. Rev. Lett. **113**, 220602 (2014).
- [12] S. Reuveni, Phys. Rev. Lett. **116**, 170601 (2016).
- [13] A. Pal, A. Kundu, M. R. Evans, J. Phys. A: Math. Theor. **49**, 225001 (2016).
- [14] A. Pal, S. Reuveni, Phys. Rev. Lett. **118**, 030603 (2017).
- [15] A. Chechkin, I. M. Sokolov, Phys. Rev. Lett. **121**, 050601 (2018).
- [16] R. G. Pinsky, preprint arXiv:1805.00320 (2018).
- [17] M. R. Evans, S. N. Majumdar, J. Phys. A: Math. Theor. **52**, 01LT01 (2019).
- [18] A. S. Bodrova, I. M. Sokolov, Phys. Rev. E **101**, 052130 (2020).
- [19] A. Pal, L. Kusmierz, S. Reuveni, Phys. Rev. Res. **2**, 043174 (2020).
- [20] R. D. Schumm, P. C. Bressloff, J. Phys. A: Math. Theor. **54**, 404004 (2021).
- [21] B. De Bruyne, S. N. Majumdar, G. Schehr, Phys. Rev. Lett. **128**, 200603 (2022).
- [22] M. Biroli, S. N. Majumdar, G. Schehr, Phys. Rev. E **107**, 064141 (2023).
- [23] B. De Bruyne, F. Mori, Phys. Rev. Research **5**, 013122 (2023).
- [24] G. García-Valladares, C. A. Plata, A. Prados, A. Manacorda, New J. Phys. **25**, 113031 (2023).
- [25] P. S. Pal, J.-M. Park, A. Pal, H. Park, J. S. Lee, Phys. Rev. E **110**, 054124 (2024).
- [26] V. Mendez, R. Flaquer-Galmés, D. Campos, Phys. Rev. E **109**, 044134 (2024).
- [27] O. Tal-Friedman, T. D. Keidar, S. Reuveni, Y. Roichman, Phys. Rev. Research **7**, 013033 (2025).
- [28] A. K. Hartmann, S. N. Majumdar, Phys. Rev. E **112**, 034102 (2025).
- [29] F. Mori, L. Mahadevan, J. R. Soc. Interface **22**, 20240677 (2025).
- [30] M. R. Evans, S. Ray, Phys. Rev. Lett. **134**, 247102 (2025).
- [31] G. Del Vecchio Del Vecchio, M. Kulkarni, S. N. Majumdar, S. Sabhapandit, arXiv:2507.05800 (2025).
- [32] A. Biswas, S. N. Majumdar, A. Pal, Phys. Rev. Lett. **135**, 227101 (2025).
- [33] M. Biroli, H. Larralde, S. N. Majumdar, and G. Schehr, Phys. Rev. Lett. **130**, 227101 (2023).
- [34] M. Magoni, F. Carollo, G. Perfetto, I. Lesanovsky, Phys. Rev. A **106**, 052210 (2022).
- [35] M. Biroli, H. Larralde, S. N. Majumdar, G. Schehr, Phys. Rev. E **109**, 014101 (2024).

- [36] M. Biroli, M. Kulkarni, S. N. Majumdar, G. Schehr, Phys. Rev. E **109**, L032106 (2024).
- [37] S. Sabhapandit, S. N. Majumdar, J. Phys. A: Math. Theor. **57**, 335003 (2024).
- [38] M. Kulkarni, S. N. Majumdar, S. Sabhapandit, J. Phys. A: Math. Theor. **58**, 105003 (2025).
- [39] N. Mesquita, S. N. Majumdar, S. Sabhapandit, J. Stat. Mech. **2025**, 103207 (2025).
- [40] D. Soldner, I. Lesanovsky, G. Perfetto, arXiv:2510.11450 (2025).
- [41] G. de Mauro, M. Biroli, S. N. Majumdar, and G. Schehr, Phys. Rev. E **113**, 014120 (2026).
- [42] D. Boyer, S. N. Majumdar, preprint arXiv:2510.21972 (2025).
- [43] M. Biroli, S. N. Majumdar, G. Schehr, arXiv:2512.00440 (2025).
- [44] M. Biroli, S. N. Majumdar, G. Schehr, Phys. Rev. E **112**, 014101 (2025).
- [45] A. Acharya, R. Majumder, S. Gupta, Phys. Rev. Lett. **135**, 127103 (2025).
- [46] R. Majumder, R. Chattopadhyay, S. Gupta, Phys. Rev. E **109**, 064137 (2024).
- [47] B. Besga, A. Bovon, A. Petrosyan, S. N. Majumdar, and S. Ciliberto, Phys. Rev. Res. **2**, 032029 (2020).
- [48] O. Tal-Friedman, A. Pal, A. Sekhon, S. Reuveni, and Y. Roichman, J. Phys. Chem. Lett. **11**, 7350 (2020).
- [49] F. Faisant, B. Besga, A. Petrosyan, S. Ciliberto, and S. N. Majumdar, J. Stat. Mech. 113203 (2021).
- [50] F. Ginot and C. Bechinger, New J. Phys. **27**, 013012 (2025).
- [51] R. Vatash and Y. Roichman, Phys. Rev. Res. **7**, L032020 (2025).
- [52] M. Biroli, S. Ciliberto, M. Kulkarni, S. N. Majumdar, A. Petrosyan, and G. Schehr, preprint arXiv:2508.07199 (2025).
- [53] See Supplemental Material.

End Matters

Fokker–Planck equation in direct space

The joint probability density $P_m(\mathbf{x}, t)$ of the N diffusing particles obeys the Fokker–Planck equation

$$\partial_t P_m(\mathbf{x}, t) = D \sum_{i=1}^N \partial_{x_i}^2 P_m(\mathbf{x}, t) - r P_m(\mathbf{x}, t) + \frac{r}{\binom{N}{m}} \sum_{S_m} \prod_{i \in S_m} \delta(x_i) P_m^{N-m}(\mathbf{x}_{S_m^c}, t), \quad (10)$$

where

$$P_m^{N-m}(\mathbf{x}_{S_m^c}, t) = \iint d\mathbf{x}_{S_m} P_m(\mathbf{x}, t) \quad (11)$$

is the $(N-m)$ -point marginal of the JPDF, with $d\mathbf{x}_{S_m} = \prod_{i \in S_m} dx_i$. The first term in the right-hand side of Eq. (10) represents standard diffusion. The loss term $-rP_m$ accounts for the probability removed at \mathbf{x} whenever a reset occurs. The third term represents batch resetting: at rate r , a uniformly chosen subset S_m of $|S_m| = m$ particles is reset to the origin, producing the factor $\prod_{i \in S_m} \delta(x_i)$, while the remaining $N-m$ coordinates retain their pre-reset distribution. We have also defined the subset $S_m^c = \{1, \dots, N\} \setminus S_m$. The vector $\mathbf{x}_{S_m^c} \in \mathbb{R}^{N-m}$, is obtained from the vector $\mathbf{x} = (x_1, \dots, x_N)$ by removing the components x_i such that $i \in S_m$, since they have been integrated out in (11). Taking the Fourier transform $\tilde{P}_m(\mathbf{k}, t) = \iint d\mathbf{x} e^{i\mathbf{k} \cdot \mathbf{x}} P_m(\mathbf{x}, t)$ of (10) one obtains

$$\partial_t \tilde{P}_m(\mathbf{k}, t) = - (Dk^2 + r) \tilde{P}_m(\mathbf{k}, t) + \frac{r}{\binom{N}{m}} \sum_{S_m} \tilde{P}_m^{N-m}(\mathbf{k}_{S_m^c}, t), \quad (12)$$

where $k^2 = |\mathbf{k}|^2 = k_1^2 + \dots + k_N^2$ and \tilde{P}_m^{N-m} is the $(N-m)$ -point marginal in Fourier space. The vector $\mathbf{k}_{S_m^c} \in \mathbb{R}^{N-m}$ is the Fourier-space counterpart of the vector $\mathbf{x}_{S_m^c}$. Using the definition of the FT of the JPDF in (1), we notice that $\tilde{P}_m^{N-m}(\mathbf{k}_{S_m^c}, t)$ can be obtained from $\tilde{P}_m(\mathbf{k}, t)$ just by setting to 0 all the components k_i of \mathbf{k} such that $i \in S_m$. This property is what allows us to derive (3) and (14). A more detailed analysis of (10) can be found in the Supplementary Material [53].

One- and two- point marginals

Setting $\partial_t \tilde{P}_m = 0$ in (12) leads to

$$\tilde{P}_m(\mathbf{k}) = \frac{\frac{r}{\binom{N}{m}} \sum_{S_m} \tilde{P}_m^{N-m}(\mathbf{k}_{S_m^c})}{r + D \sum_{i=1}^N k_i^2}. \quad (13)$$

This expression relates the Fourier transform of the NESS for a general m to the Fourier transform of its marginals. Since the equation is valid for any vector \mathbf{k} , we can choose to calculate it in $\mathbf{k} = (k, 0, \dots, 0)$ in order to obtain a closed equation for $\tilde{P}_m(\mathbf{k} = (k, 0, \dots, 0))$, which, as noted above, coincides with the Fourier transform of the one-point marginal $\tilde{P}_m^1(k)$. This closed equation can be solved and the Fourier transform inverted to obtain (5). Repeating the same argument, we can evaluate (12) in $(k_1, k_2, 0, \dots, 0)$, which gives an expression involving only $\tilde{P}_m^1(k)$ and $\tilde{P}_m^2(k_1, k_2)$. Since we already know $\tilde{P}_m^1(k)$, we can solve for $\tilde{P}_m^2(k_1, k_2)$ and then invert the Fourier transform. This procedure leads to

$$\tilde{P}_m^2(k_1, k_2) = \frac{(2-\beta) + (\beta-1)[\tilde{P}_m^1(k_1) + \tilde{P}_m^1(k_2)]}{\beta + \ell_m^2(k_1^2 + k_2^2)}, \quad \beta = \frac{2N-m-1}{N-1}, \quad (14)$$

which in real space takes the scaling form

$$P_m^2(x_1, x_2) = \frac{1}{\ell_m^2} \mathcal{P}_\beta\left(\frac{x_1}{\ell_m}, \frac{x_2}{\ell_m}\right). \quad (15)$$

The function $\mathcal{P}_\beta(u, v)$ is expressed as

$$\begin{aligned}\mathcal{P}_\beta(u, v) = & \frac{2-\beta}{2\pi} K_0\left(\sqrt{\beta}\sqrt{u^2+v^2}\right) + \frac{\beta-1}{4\pi} \left[\int_{-\infty}^{\infty} dz e^{-|z|} K_0\left(\sqrt{\beta}\sqrt{(u-z)^2+v^2}\right) \right. \\ & \left. + \int_{-\infty}^{\infty} dz e^{-|z|} K_0\left(\sqrt{\beta}\sqrt{u^2+(v-z)^2}\right) \right],\end{aligned}\quad (16)$$

where $\beta = \frac{2N-m-1}{N-1}$ and $K_0(z)$ is the modified Bessel function of the second kind of order zero.

Derivations of the correlation functions

The functions $\mathcal{C}_1(t)$, $\mathcal{C}_2(t)$ and $a(t; m, N)$ defined in (6) and (7) can be computed in two ways. (i) One may multiply Eq. (10) by an arbitrary observable $f(\mathbf{x})$ and integrate over all configurations \mathbf{x} , which yields a differential equation for $\langle f(\mathbf{x}) \rangle$. Solving this equation for specific choices such as $f(\mathbf{x}) = x_i^2 x_j^2$, x_i^2 , or x_i^4 directly provides the required moments. (ii) Alternatively, one may work in Fourier space: starting from Eq. (12), and using the same reasoning that leads to (14), one obtains the full time-dependent expressions for the marginals $\tilde{P}_1(k, t)$ and $\tilde{P}_2(k_1, k_2, t)$, from which all desired moments follow by differentiation:

$$\langle x_i^2(t) \rangle = - \frac{\partial^2 \tilde{P}_1(k, t)}{\partial k^2} \Big|_{k=0}, \quad \langle x_i^4(t) \rangle = \frac{\partial^4 \tilde{P}_1(k, t)}{\partial k^4} \Big|_{k=0}, \quad \langle x_i^2 x_j^2(t) \rangle = \frac{\partial^2}{\partial k_1^2} \frac{\partial^2}{\partial k_2^2} \tilde{P}_2(k_1, k_2, t) \Big|_{k_1, k_2=0}. \quad (17)$$

Defining $\tilde{r} = \frac{m}{N} r$ and $\beta = \frac{2N-m-1}{N-1}$ it is then straightforward to get

$$\mathcal{C}_1(t) = \frac{4D^2}{\tilde{r}^2} f_1(\tilde{r}t), \quad f_1(z) = 5 - 4e^{-z} - 6ze^{-z} - e^{-2z}, \quad (18)$$

$$\mathcal{C}_2(t) = \frac{4D^2}{\tilde{r}^2} f_2(\tilde{r}t; \beta), \quad f_2(z; \beta) = 2\left(\frac{1-e^{-\beta z}}{\beta} - \frac{e^{-z} - e^{-\beta z}}{\beta-1}\right) - 1 - e^{-2z} + 2e^{-z}, \quad (19)$$

$$a(t; m, N) = A(\tilde{r}t; \beta), \quad A(z; \beta) = \frac{f_2(z; \beta)}{f_1(z)}. \quad (20)$$

The function $f_2(z; \beta)$ has a diverging factor when $\beta \rightarrow 1$ ($m \rightarrow N$), but setting $\beta = 1 + \epsilon$ and taking the limit $\epsilon \rightarrow 0$ recovers the known result for the fully synchronous case $f_2(z; 1) = 1 - 2ze^{-z} - e^{-2z}$ [41]. A more detailed analysis of these quantities can be found in [53].

Maximum of $A(z; \beta)$

The asymptotic expansions of the maximum $z^*(\beta)$ can be obtained by analyzing the extremum condition $\partial_z A(z; \beta) = F(z, \beta) = 0$, where $\beta = \frac{2N-m-1}{N-1}$. When $\beta \rightarrow 1^+$, we can define $\beta = 1 + \epsilon$ where $\epsilon = \frac{N-m}{N-1}$. Since $z^*(\beta = 1 + \epsilon) \rightarrow \infty$ as $\epsilon \rightarrow 0$, we must consider the joint limit $z \rightarrow \infty$, $\epsilon \rightarrow 0$, while keeping the product $z\epsilon$ finite and expand $F(z, 1 + \epsilon)$ within this double-scaling regime, retaining only the leading terms. We then introduce the asymptotic ansatz $z^*(\epsilon) = \frac{a_0}{\epsilon} + a_1$, insert it into the extremum condition, expand for small ϵ , and set to zero the coefficients at successive orders. This yields the coupled equations

$$e^{a_0}(5 - 3a_0) = 5, \quad e^{a_0}[(5 - 3a_0)(a_1 - 1) + 6 - 3a_1] = 5. \quad (21)$$

Solving them gives $a_0 = 1.1262\dots$ and $a_1 = 2$. Therefore, in the limit $\epsilon \rightarrow 0$, the position of the maximum diverges as $z^*(\epsilon) \simeq \frac{1.1262}{\epsilon} + 2$.

The opposite limit $\beta \rightarrow 2^-$ can be obtained by setting $\beta = 2 - \delta$ in (20), where $\delta = \frac{m-1}{N-1}$, and expanding the resulting expression to first order in δ . Differentiating this expansion with respect to z and imposing the extremum condition then yields

$$6e^z z^2 + 13e^z z - 10e^{2z} z - 3e^{3z} z + 13e^z - 23e^{2z} + 11e^{3z} - 1 = 0, \quad (22)$$

Solving this equation numerically gives the limiting value $\bar{z} = 2.6495\dots$. See also the SM [53].

Supplemental Material for
Tuning the strength of emergent correlations in a Brownian gas via batch resetting

Gabriele de Mauro,¹ Satya N. Majumdar,¹ and Gr  gory Schehr²

¹*LPTMS, CNRS, Universit   Paris-Saclay, 91405 Orsay, France*

²*Sorbonne Universit  , Laboratoire de Physique Th  orique et Hautes Energies,
CNRS UMR 7589, 4 Place Jussieu, 75252 Paris Cedex 05, France*

Contents

S1. Illustrative example: $N = 3$ and $m = 2$	2
S2. Fokker–Planck equation for arbitrary m and N	4
S3. One- and two-point marginals	6
S4. JPDF for $m = N - 1$	7
S5. JPDF for $m = 1$	8
S6. Correlators: $\mathcal{C}_2(t)$ and $a(t; m, N)$	8
S6.1. Analysis of the maximum $z^*(\beta)$ of $A(z; \beta)$	10
S6.2. Stationary correlators	11
S7. Physical interpretation of the maximum of $A(z; \beta)$	13
S8. Connected pair correlation function	14
S9. Spectral form factor	16
S10. Generalization to higher dimensions d	17
S10.1. Correlations	18
References	20

S1. ILLUSTRATIVE EXAMPLE: $N = 3$ AND $m = 2$

As a first instructive example, we consider a system of $N = 3$ particles in which $m = 2$ of them are reset at each reset event, with a constant rate r . Then, in the next section, we generalize the problem to arbitrary values of m and N . The evolution of the joint probability density (JPDF) $P_{m=2}(x_1, x_2, x_3, t)$ is governed by the Fokker–Planck equation

$$\begin{aligned} \frac{\partial}{\partial t} P_{m=2}(x_1, x_2, x_3, t) &= D \sum_{i=1}^3 \frac{\partial^2}{\partial x_i^2} P_{m=2}(x_1, x_2, x_3, t) - r P_{m=2}(x_1, x_2, x_3, t) \\ &\quad + \frac{r}{3} \left[\delta(x_1) \delta(x_2) \int_{-\infty}^{\infty} dy_1 dy_2 P_{m=2}(y_1, y_2, x_3, t) \right. \\ &\quad \left. + \delta(x_1) \delta(x_3) \int_{-\infty}^{\infty} dy_1 dy_3 P_{m=2}(y_1, x_2, y_3, t) \right. \\ &\quad \left. + \delta(x_2) \delta(x_3) \int_{-\infty}^{\infty} dy_2 dy_3 P_{m=2}(x_1, y_2, y_3, t) \right]. \end{aligned} \quad (\text{S1})$$

The first term on the right-hand side of (S1) describes the independent diffusion of the three particles with diffusion coefficient D . The second term is a loss term accounting for the fact that, with rate r , a reset event occurs and the system leaves the configuration $\mathbf{x} = (x_1, x_2, x_3)$. The remaining terms in the square brackets represent the gain due to reset events. At each reset, two particles out of three are chosen uniformly at random, hence each of the three possible pairs is selected with probability $1/3$. For instance, the contribution

$$\frac{r}{3} \delta(x_1) \delta(x_2) \int_{-\infty}^{\infty} dy_1 dy_2 P_{m=2}(y_1, y_2, x_3, t) \quad (\text{S2})$$

corresponds to events where particles 1 and 2 are reset to the origin. The Dirac delta functions $\delta(x_1)\delta(x_2)$ enforce that they are brought at $x_1 = x_2 = 0$, while the integral over y_1, y_2 sums over all possible pre-reset positions of these two particles, keeping particle 3 fixed at x_3 . The other two terms in the brackets are interpreted in the same way, with the roles of the three particles permuted. It is convenient to take a Fourier transform (FT) of Eq. (S1), defining

$$\tilde{P}_{m=2}(k_1, k_2, k_3, t) = \iint d\mathbf{x} e^{i\mathbf{k}\cdot\mathbf{x}} P_{m=2}(x_1, x_2, x_3, t), \quad \mathbf{k} = (k_1, k_2, k_3), \quad (\text{S3})$$

which gives

$$\begin{aligned} \frac{\partial}{\partial t} \tilde{P}_{m=2}(k_1, k_2, k_3, t) &= -D (k_1^2 + k_2^2 + k_3^2) \tilde{P}_{m=2}(k_1, k_2, k_3, t) - r \tilde{P}_{m=2}(k_1, k_2, k_3, t) \\ &\quad + \frac{r}{3} \left[\tilde{P}_{m=2}(0, 0, k_3, t) + \tilde{P}_{m=2}(0, k_2, 0, t) + \tilde{P}_{m=2}(k_1, 0, 0, t) \right]. \end{aligned} \quad (\text{S4})$$

We now introduce the one-point marginal

$$P_{m=2}^1(x, t) = \int_{-\infty}^{\infty} dx_2 \int_{-\infty}^{\infty} dx_3 P_{m=2}(x, x_2, x_3, t), \quad (\text{S5})$$

and its FT

$$\tilde{P}_{m=2}^1(k_1, t) = \int_{-\infty}^{\infty} dx_1 e^{ik_1 x_1} P_{m=2}^1(x_1, t) = \tilde{P}_{m=2}^1(k_1, 0, 0, t). \quad (\text{S6})$$

The last equality in (S6) follows directly from the definition of the FT in (S3). Indeed, setting a component $k_i = 0$ in (S3) is equivalent to marginalizing the JPDF $P_m(x_1, x_2, x_3)$ over the corresponding spatial variable x_i . As a result, once the FT of the full JPDF, $\tilde{P}_{m=2}(k_1, k_2, k_3, t)$, is known, the FT of any marginal distribution can be obtained simply by setting the appropriate components k_i to zero. Since all particles play the same role in the dynamics, we also have $\tilde{P}_{m=2}^1(k, t) = \tilde{P}_{m=2}^1(0, k, 0, t) = \tilde{P}_{m=2}^1(0, 0, k, t)$. This observation will be repeatedly used in the following sections to derive closed equations for the marginal distributions. Using the definitions in (S5) and (S6) we can rewrite (S1)

and (S8) respectively as

$$\begin{aligned} \frac{\partial}{\partial t} P_{m=2}(x_1, x_2, x_3, t) &= D \sum_{i=1}^3 \frac{\partial^2}{\partial x_i^2} P_{m=2}(x_1, x_2, x_3, t) - r P_{m=2}(x_1, x_2, x_3, t) \\ &+ \frac{r}{3} \left[\delta(x_1) \delta(x_2) P_{m=2}^1(x_3, t) + \delta(x_1) \delta(x_3) P_{m=2}^1(x_2, t) + \delta(x_2) \delta(x_3) P_{m=2}^1(x_1, t) \right], \end{aligned} \quad (\text{S7})$$

and

$$\frac{\partial}{\partial t} \tilde{P}_{m=2}(k_1, k_2, k_3, t) = - (r + D|k|^2) \tilde{P}_{m=2}(k_1, k_2, k_3, t) + \frac{r}{3} \left[\tilde{P}_{m=2}^1(k_3, t) + \tilde{P}_{m=2}^1(k_2, t) + \tilde{P}_{m=2}^1(k_1, t) \right], \quad (\text{S8})$$

where $|k|^2 = k_1^2 + k_2^2 + k_3^2$. By setting the time derivative in (S8) to zero, we can obtain an equation for the stationary JPDF in Fourier space, namely

$$\tilde{P}_{m=2}(k_1, k_2, k_3) = \frac{\frac{r}{3} \left[\tilde{P}_{m=2}^1(k_1) + \tilde{P}_{m=2}^1(k_2) + \tilde{P}_{m=2}^1(k_3) \right]}{r + D(k_1^2 + k_2^2 + k_3^2)}. \quad (\text{S9})$$

Using the observation made above, namely that setting components of \mathbf{k} to zero in the Fourier-transformed JPDF yields the FT of the corresponding marginals, we can now evaluate (S9) at $\mathbf{k} = (k, 0, 0)$. This gives a closed equation for the one-point marginal

$$\tilde{P}_{m=2}^1(k) = \frac{\frac{r}{3} \left[2 + \tilde{P}_{m=2}^1(k) \right]}{D k^2 + r}. \quad (\text{S10})$$

Solving for $\tilde{P}_{m=2}^1(k)$ yields

$$\tilde{P}_{m=2}^1(k) = \frac{1}{1 + \ell_2^2 k^2}, \quad \ell_2 = \sqrt{\frac{3D}{2r}}. \quad (\text{S11})$$

By inverting the FT, we obtain

$$P_{m=2}^1(x) = \frac{1}{2\pi} \int_{-\infty}^{\infty} dk e^{-ikx} \tilde{P}_{m=2}^1(k) = \frac{1}{\ell_2} \mathcal{R}\left(\frac{x}{\ell_2}\right), \quad \mathcal{R}(u) = \frac{1}{2} e^{-|u|}. \quad (\text{S12})$$

We can proceed similarly by evaluating (S9) at $\mathbf{k} = (k_1, k_2, 0)$. Defining the two-point marginal in Fourier space as $\tilde{P}_{m=2}^2(k_1, k_2) \equiv \tilde{P}_{m=2}(k_1, k_2, 0)$, we get

$$\tilde{P}_{m=2}^2(k_1, k_2) = \frac{\frac{r}{3} \left[\tilde{P}_{m=2}^1(k_1) + \tilde{P}_{m=2}^1(k_2) + 1 \right]}{r + D(k_1^2 + k_2^2)}, \quad (\text{S13})$$

which is a closed equation, since $\tilde{P}_{m=2}^1(k)$ is already known from (S11). To invert the FT in (S13), we use the identity

$$\frac{1}{(2\pi)^2} \int_{-\infty}^{\infty} dk_1 \int_{-\infty}^{\infty} dk_2 \frac{e^{-i(k_1 x_1 + k_2 x_2)}}{r + D(k_1^2 + k_2^2)} = \frac{1}{2\pi D} K_0\left(\sqrt{\frac{r}{D}} \sqrt{x_1^2 + x_2^2}\right), \quad (\text{S14})$$

where $K_0(z)$ is the modified Bessel function of the second kind of order 0. This relation leads to

$$\begin{aligned} P_{m=2}^2(x_1, x_2) &= \frac{r}{3} \frac{1}{2\pi D} K_0\left(\sqrt{\frac{r}{D}} \sqrt{x_1^2 + x_2^2}\right) \\ &+ \frac{r}{3} \frac{1}{2\pi D} \int_{-\infty}^{\infty} \frac{dy}{2\ell_2} e^{-|y|/\ell_2} K_0\left(\sqrt{\frac{r}{D}} \sqrt{(x_1 - y)^2 + x_2^2}\right) \\ &+ \frac{r}{3} \frac{1}{2\pi D} \int_{-\infty}^{\infty} \frac{dy}{2\ell_2} e^{-|y|/\ell_2} K_0\left(\sqrt{\frac{r}{D}} \sqrt{x_1^2 + (x_2 - y)^2}\right). \end{aligned} \quad (\text{S15})$$

In the following sections, we show that these one- and two-point marginals can always be obtained for arbitrary m and N , while the full stationary state takes a particularly simple form only in the cases $m = 1$ and $m = N - 1$, in addition

to the known case $m = N$ [1]. Here, with the specific choice $N = 3$ and $m = 2$, the JPDF in Fourier space can be obtained by inserting (S11) into (S9):

$$\tilde{P}_{m=2}(k_1, k_2, k_3) = \frac{1}{3} \frac{r}{r + D(k_1^2 + k_2^2 + k_3^2)} \sum_{j=1}^3 \frac{1}{1 + \ell_2^2 k_j^2}, \quad \ell_2 = \sqrt{\frac{3D}{2r}}. \quad (\text{S16})$$

We now notice that

$$\mathcal{F}^{-1} \left[\frac{1}{1 + \ell^2 \sum_{i=1}^3 k_i^2} \right] = \frac{1}{\ell^3} \frac{1}{(2\pi)^{3/2}} \left(\frac{|\mathbf{x}|}{\ell} \right)^{-\nu} K_\nu \left(\frac{|\mathbf{x}|}{\ell} \right) = P_{m=3}(\mathbf{x}), \quad \ell = \sqrt{\frac{D}{r}}, \quad \nu = \frac{1}{2}, \quad (\text{S17})$$

where \mathcal{F}^{-1} denotes the inverse FT, $|\mathbf{x}| = \sqrt{x_1^2 + x_2^2 + x_3^2}$ and $K_\nu(z)$ is the modified Bessel function of the second kind of order ν . This expression is precisely the stationary state $P_{m=3}(\mathbf{x})$ of a system of $N = 3$ particles that are all simultaneously reset ($m = 3$) [1]. We can now use the identity

$$K_{1/2}(z) = \sqrt{\frac{\pi}{2z}} e^{-z} \quad (\text{S18})$$

to rewrite Eq. (S17) as

$$P_{m=3}(\mathbf{x}) = \frac{1}{\ell^3} \frac{1}{4\pi} \left(\frac{|\mathbf{x}|}{\ell} \right)^{-1} e^{-|\mathbf{x}|/\ell}. \quad (\text{S19})$$

In addition, the sum in (S16) contains terms that are exactly the one-point marginal in Fourier space $\tilde{P}_{m=2}^1(k_j)$, and therefore their inverse FT gives (S11). Using these observations and the convolution property of the FT, the JPDF can be written as

$$\begin{aligned} P_{m=2}(x_1, x_2, x_3) &= \frac{1}{3} \int_{-\infty}^{\infty} dy P_{m=2}^1(x_1 - y) P_{m=3}(y, x_2, x_3) \\ &+ \frac{1}{3} \int_{-\infty}^{\infty} dy P_{m=2}^1(x_2 - y) P_{m=3}(x_1, y, x_3) \\ &+ \frac{1}{3} \int_{-\infty}^{\infty} dy P_{m=2}^1(x_3 - y) P_{m=3}(x_1, x_2, y). \end{aligned} \quad (\text{S20})$$

This shows that, for $N = 3$ and $m = 2$, the stationary JPDF can be written as a sum of convolutions between the one-point marginal $P_{m=2}^1$ and the fully synchronous JPDF $P_{m=3}$. Physically, the system behaves as if the dynamics were fully synchronous, except that at each resetting event one particle is effectively replaced by an independent particle drawn from its stationary one-body distribution. All three possible choices of the pair of particles to be reset occur with equal probability, resulting in the prefactor $1/3$. This construction naturally generalizes to arbitrary N in the case $m = N - 1$, as expressed in Eq. (S43) below.

S2. FOKKER-PLANCK EQUATION FOR ARBITRARY m AND N

In this section, we show that the structure uncovered in the illustrative case $N = 3$ and $m = 2$ naturally extends to arbitrary values of m and N . We now consider the JPDF $P_m(\mathbf{x}, t)$, where $\mathbf{x} = \{x_1, \dots, x_N\}$ are the positions of the N particles. Each particle performs an independent Brownian motion with diffusion constant D , and, at Poissonian times with rate r , a subset of exactly m particles is reset to the origin. We define the n -point marginals of the JPDF in direct and Fourier space, respectively as

$$\begin{aligned} P_m^n(x_1, \dots, x_n, t) &= \iint_{-\infty}^{\infty} dx_{n+1} \dots dx_N P_m(\mathbf{x}, t), \\ \tilde{P}_m^n(k_1, \dots, k_n, t) &= \iint_{-\infty}^{\infty} dx_1 \dots dx_n e^{i(k_1 x_1 + \dots + k_n x_n)} P_m^n(x_1, \dots, x_n, t). \end{aligned} \quad (\text{S21})$$

The time evolution of $P_m(\mathbf{x}, t)$ is governed by the Fokker–Planck equation

$$\partial_t P_m(\mathbf{x}, t) = D \sum_{i=1}^N \partial_{x_i}^2 P_m(\mathbf{x}, t) - r P_m(\mathbf{x}, t) + \frac{r}{\binom{N}{m}} \sum_{S_m} \prod_{i \in S_m} \delta(x_i) P_m^{N-m}(\mathbf{x}_{S_m^c}, t) \quad (\text{S22})$$

where

$$P_m^{N-m}(\mathbf{x}_{S_m^c}, t) = \iint d\mathbf{x}_{S_m} P_m(\mathbf{x}, t) \quad (\text{S23})$$

is the $(N - m)$ -point marginal, as defined in (S21). The notation $\iint d\mathbf{x}_{S_m}$ indicates that we are integrating over all the components x_i such that $i \in S_m$, where S_m is a subset $S_m \subseteq \{1, \dots, N\}$ such that $|S_m| = m$. It follows that P_m^{N-m} only depends on the components x_i of \mathbf{x} such that $i \notin S_m$, or, equivalently, such that $i \in S_m^c$ where S_m^c is the set $S_m^c = \{1, \dots, N\} \setminus S_m$. We compactly denote the remaining components as $\mathbf{x}_{S_m^c} \in \mathbb{R}^{N-m}$. To be clearer, we consider again the case $N = 3$ and $m = 2$. This means $P_m^{N-m} \rightarrow P_2^1$ and $S_m \rightarrow S_2$. In this case, there are three possibilities for the set S_2 . For example we may have $S_m = \{1, 2\}$, which implies $S_m^c = \{3\}$. Then (S23) becomes

$$P_2^1(\mathbf{x}_{S_2^c} = x_3, t) = \iint d\mathbf{x}_{S_2} P_2(\mathbf{x}, t) = \iint dx_1 dx_2 P_2(\mathbf{x}, t) \quad (\text{S24})$$

With the choices $S_2 = \{2, 3\}$ and $S_2 = \{1, 3\}$ we obtain instead, respectively, $P_2^1(\mathbf{x}_{S_2^c} = x_1, t)$ and $P_2^1(\mathbf{x}_{S_2^c} = x_2, t)$. The sum \sum_{S_m} runs over all the possible subsets S_m . Since all particles play the same role in the dynamics, the three functions $P_2^1(x_1, t)$, $P_2^1(x_2, t)$ and $P_2^1(x_3, t)$ all have the same functional form.

We now analyze the terms appearing in the right hand side of (S22). The first term represents standard diffusion with diffusion constant D . The second term accounts for the loss of probability at position \mathbf{x} due to the resetting events occurring at rate r . Whenever a resetting happens, some of the particles currently at \mathbf{x} are reset to the origin, thus reducing the probability at that point. The last term captures the effect of batch resetting, and it generalizes the terms in the square bracket of (S1). Each time a reset occurs, a random subset $S_m \subseteq \{1, \dots, N\}$ made of $|S_m| = m$ particles is selected from the N particles. This selection is uniform, meaning that any subset of size m is equally likely to be chosen. The contribution to the probability density from resetting these m particles is given by $\prod_{i \in S_m} \delta(x_i)$, where the Dirac delta $\delta(x_i)$ forces the positions of the selected particles to reset to the origin. The remaining $N - m$ particles are unaffected by the resetting event and continue to evolve according to their diffusion dynamics. Therefore, we must multiply by the marginal distribution of the positions of these $N - m$ particles, namely $P_m^{N-m}(\mathbf{x}_{S_m^c}, t)$. The factor $1/\binom{N}{m}$ is the probability of selecting a particular subset, since any subset S of size m is equally probable. We then sum over all possible subsets S_m to account for all possible choices of particles to reset. Finally, we multiply the probability of a resetting event occurring per unit time, which is simply the rate r .

It is now convenient to take a FT of (S22), which leads to

$$\partial_t \tilde{P}_m(\mathbf{k}, t) = -(Dk^2 + r) \tilde{P}_m(\mathbf{k}, t) + \frac{r}{\binom{N}{m}} \sum_{S_m} \tilde{P}_m^{N-m}(\mathbf{k}_{S_m^c}, t), \quad (\text{S25})$$

where we have defined

$$\tilde{P}_m(\mathbf{k}, t) = \iint d\mathbf{x} e^{i\mathbf{k} \cdot \mathbf{x}} P_m(\mathbf{x}, t). \quad (\text{S26})$$

and $k^2 = |\mathbf{k}|^2 = k_1^2 + \dots + k_N^2$. The function $\tilde{P}_m^{N-m}(\mathbf{k}_{S_m^c}, t)$ denotes the $(N - m)$ -dimensional FT of the marginal distribution $P_m^{N-m}(\mathbf{x}_{S_m^c}, t)$. For instance, when $N = 3$ and $m = 2$, one possible choice is $S_2 = \{1, 2\}$, which implies $S_2^c = \{3\}$. In this case, $\mathbf{k}_{S_2^c} = (k_3)$ and

$$\tilde{P}_m^{N-m}(\mathbf{k}_{S_m^c}, t) = \tilde{P}_2^1(k_3, t) = \int_{-\infty}^{\infty} dx_3 e^{ik_3 x_3} P_2^1(x_3, t). \quad (\text{S27})$$

It is important to note that the Fourier-space marginal $\tilde{P}_2^1(k_3, t)$ can equivalently be obtained from the full Fourier-transformed JPDF $\tilde{P}_2(\mathbf{k}, t)$ by evaluating it at $\mathbf{k} = (0, 0, k_3)$, or, by symmetry, at $(k_3, 0, 0)$ or $(0, k_3, 0)$. This follows directly from the definition (S26): setting a component $k_i = 0$ corresponds to marginalizing the direct space JPDF over the associated spatial coordinate x_i . The same argument extends to higher-order marginals: by setting n components of \mathbf{k} to zero in the full Fourier-transformed JPDF, one directly obtains the FT of the corresponding $(N - n)$ -point marginal. This observation will prove useful in the following sections. Finally, one can readily check that setting $N = 3$ and $m = 2$ in (S25) reproduces (S8).

S3. ONE- AND TWO-POINT MARGINALS

From (S25) we can derive an expression for the stationary state of the system. By setting the temporal derivative to zero, we obtain:

$$\tilde{P}_m(\mathbf{k}) = \frac{\frac{r}{\binom{N}{m}} \sum_{S_m} \tilde{P}_m^{N-m}(\mathbf{k}_{S_m^c})}{r + D \sum_{i=1}^N k_i^2}. \quad (\text{S28})$$

This equation can, in principle, be used to determine the full JPDF of the system and its marginals for all values of m . Specifically, since (S28) holds for any vector \mathbf{k} , we can evaluate it at any convenient value. Using the observation made above that setting components of \mathbf{k} to zero in $\tilde{P}_m(\mathbf{k})$ yields Fourier-space marginals, we may choose $\mathbf{k} = (k, 0, \dots, 0)$. Doing this, the left-hand side becomes just the FT $\tilde{P}_m^1(k)$ of the one-point marginal defined in (S21). In this case, the right-hand side will depend only on $\tilde{P}_m^1(k)$, allowing us to derive the following expression:

$$\tilde{P}_m^1(k) = \frac{1}{1 + \ell_m^2 k^2} \quad \tilde{r} = \frac{m}{N} r \quad \text{and} \quad \ell_m^2 = \frac{D}{\tilde{r}}. \quad (\text{S29})$$

Next, we apply the same reasoning to derive the two-point marginal. We evaluate (S28) at $\mathbf{k} = (k_1, k_2, 0, \dots, 0)$. With this choice, the left-hand side of (S28) reduces to the FT of the two-point marginal, $\tilde{P}_m^2(k_1, k_2)$. On the right-hand side, the sum over subsets S_m produces contributions that depend on how the indices 1 and 2 are distributed with respect to S_m . Specifically, depending on whether neither of the indices 1, 2 belongs to S_m , exactly one of them belongs to S_m , or both belong to S_m , the corresponding terms are respectively proportional to $\tilde{P}_m^2(k_1, k_2)$, to $\tilde{P}_m^1(k_1)$ or $\tilde{P}_m^1(k_2)$, or to a constant. This classification allows us to express (S28) as a closed equation involving only the known one-point marginal and the unknown two-point marginal, from which $\tilde{P}_m^2(k_1, k_2)$ can be obtained explicitly as

$$\tilde{P}_m^2(k_1, k_2) = \frac{(2 - \beta) + (\beta - 1) [\tilde{P}_m^1(k_1) + \tilde{P}_m^1(k_2)]}{\beta + \ell_m^2 (k_1^2 + k_2^2)}, \quad \beta = \frac{2N - m - 1}{N - 1}. \quad (\text{S30})$$

In principle, repeating this argument allows one to obtain all the marginals up to the full JPDF in Fourier space. However, their expressions quickly become complex for marginals involving more than two particles. The FT in Equations (S29) and (S30) can be inverted to obtain:

$$P_m^1(x) = \frac{1}{\ell_m} \mathcal{R}\left(\frac{x}{\ell_m}\right), \quad \mathcal{R}(u) = \frac{1}{2} e^{-|u|}, \quad (\text{S31})$$

and

$$P_m^2(x_1, x_2) = (2 - \beta) h(x_1, x_2) + (\beta - 1) [I(x_1, x_2) + I(x_2, x_1)], \quad (\text{S32})$$

where

$$h(x_1, x_2) = \frac{1}{2\pi\ell_m^2} K_0\left(\sqrt{\beta} \sqrt{\left(\frac{x_1}{\ell_m}\right)^2 + \left(\frac{x_2}{\ell_m}\right)^2}\right), \quad \ell_m = \sqrt{\frac{D}{\tilde{r}}}, \quad (\text{S33})$$

$$I(x_1, x_2) = (P_1 *_1 h)(x_1, x_2) = \int_{-\infty}^{\infty} \frac{dy}{2\ell_m} e^{-|y|/\ell_m} h(x_1 - y, x_2), \quad (\text{S34})$$

and $K_0(z)$ is the modified Bessel function of the second kind of order zero. The symbol $*_1$ indicates a convolution over the first coordinate. It is useful to observe that the parameters $\beta - 1$ and $2 - \beta$ admit a simple probabilistic interpretation. Fix two particles i and j and condition on particle i being reset during a given event. Since the remaining $m - 1$ particles are chosen uniformly among the other $N - 1$, the probability that particle j is also reset is

$$2 - \beta = \frac{m - 1}{N - 1},$$

while the complementary probability that particle j is not reset is

$$\beta - 1 = \frac{N - m}{N - 1}.$$

These two probabilities sum to unity and directly determine the relative weights of the different contributions in (S30). In particular, the coefficient $2 - \beta$ multiplies the contribution associated with the simultaneous resetting of both particles; accordingly, the function $h(x_1, x_2)$ has the same functional form as the stationary joint distribution in the fully synchronous case [1]. Conversely, the coefficient $\beta - 1$ weighs the contributions arising from events in which only one of the two particles is reset, which can be interpreted similarly to (S20).

We can rewrite the function $P_2(x_1, x_2)$ in the scaling form

$$P_2(x_1, x_2) = \frac{1}{\ell_m^2} \mathcal{P}_\beta \left(\frac{x_1}{\ell_m}, \frac{x_2}{\ell_m} \right), \quad (\text{S35})$$

where the scaling function is given by

$$\begin{aligned} \mathcal{P}_\beta(u, v) = & \frac{2 - \beta}{2\pi} K_0 \left(\sqrt{\beta} \sqrt{u^2 + v^2} \right) \\ & + \frac{\beta - 1}{4\pi} \left[\int_{-\infty}^{\infty} dz e^{-|z|} K_0 \left(\sqrt{\beta} \sqrt{(u - z)^2 + v^2} \right) \right. \\ & \left. + \int_{-\infty}^{\infty} dz e^{-|z|} K_0 \left(\sqrt{\beta} \sqrt{u^2 + (v - z)^2} \right) \right]. \end{aligned} \quad (\text{S36})$$

The function $\mathcal{P}_\beta(0, v)$ behaves as

$$\mathcal{P}_\beta(0, v) \simeq \begin{cases} -\frac{2-\beta}{2\pi} \ln \left(\frac{\sqrt{\beta}}{2} |v| \right), & v \rightarrow 0, \\ \frac{\sqrt{\beta-1}}{4} e^{-v}, & v \rightarrow \infty. \end{cases} \quad (\text{S37})$$

Integrating over one of the two variables, we recover the one-point marginal

$$\int dv \mathcal{P}_\beta(u, v) = \mathcal{R}(u) = \frac{1}{2} e^{-|u|}. \quad (\text{S38})$$

Setting $m = N$, which means $\beta = 1$, we recover the known result for N particles that are all reset simultaneously [1]:

$$\mathcal{P}_\beta(u, v) = \frac{1}{2\pi} K_0 \left(\sqrt{u^2 + v^2} \right). \quad (\text{S39})$$

We observe that the scaling function $\mathcal{R}(u)$ does not depend on m for any value of N . However, the situation changes for the joint function $\mathcal{P}_\beta(u, v)$: as soon as $m \neq N$ ($\beta \neq 1$), additional terms appear in (S36). This implies that one-particle observables, such as the density profile, retain the same qualitative form as in the fully synchronous case, whereas any observable involving two particles is qualitatively modified when $m \neq N$. This is precisely what happens for the two-point correlators studied below and in the Letter.

S4. JPDF FOR $m = N - 1$

For the case $m = N - 1$, it is possible to obtain an explicit expression of the full stationary state $P_{N-1}(\mathbf{x})$, and not only for its first two marginals. Starting from (S28), one can directly set $m = N - 1$, which leads to an expression involving only the one-point marginal. Since we have already found the one-point marginal in general for any m (see (S31)) we get

$$\tilde{P}_{N-1}(\mathbf{k}) = \frac{r}{D \sum_{i=1}^N k_i^2 + r} \frac{1}{N} \sum_{j=1}^N \frac{\tilde{r}}{D k_j^2 + \tilde{r}}, \quad m = N - 1, \quad (\text{S40})$$

where $\tilde{r} = \frac{N-1}{N} r$. To invert the FT in (S40), we notice that

$$\mathcal{F}^{-1}\left[\frac{r}{D\sum_i k_i^2 + r}\right] = \frac{1}{\ell^N} \frac{1}{(2\pi)^{N/2}} \left(\frac{|\mathbf{x}|}{\ell}\right)^{-\nu} K_\nu\left(\frac{|\mathbf{x}|}{\ell}\right) = P_{m=N}(\mathbf{x}), \quad (\text{S41})$$

where \mathcal{F}^{-1} indicates the inverse FT, $K_\nu(z)$ is the modified Bessel function of the second kind of order ν , $|\mathbf{x}| = \sqrt{x_1^2 + \dots + x_N^2}$, $\ell = \sqrt{D/r}$ and $\nu = \frac{N}{2} - 1$. The function $P_{m=N}(\mathbf{x})$ is exactly the JPDF of a batch resetting system of N particles which are all simultaneously reset (i.e. with $m = N$)^[1]. We also define

$$F_j(\mathbf{x}) = \mathcal{F}^{-1}\left[\frac{\tilde{r}}{Dk_j^2 + \tilde{r}}\right] = \frac{1}{2\ell_{N-1}} e^{-|x_j|/\ell_{N-1}} \prod_{i \neq j} \delta(x_i) = \frac{1}{\ell_{N-1}} \mathcal{R}\left(\frac{|x_j|}{\ell_{N-1}}\right) \prod_{i \neq j} \delta(x_i), \quad \ell_{N-1} = \sqrt{\frac{ND}{(N-1)r}}. \quad (\text{S42})$$

Interestingly, in the above expression appears the one-point marginal (i.e. the average density of particles) $P_{m=N-1}^1(x_j) = \frac{1}{\ell_{N-1}} \mathcal{R}\left(\frac{|x_j|}{\ell_{N-1}}\right)$ of our system with $m = N - 1$ (see (S31)). Equations (S41) and (S42), together with the convolution property of the FT, allow us to express the JPDF $P_{N-1}(\mathbf{x})$ as

$$P_{N-1}(\mathbf{x}) = \frac{1}{N} \sum_{j=1}^N (P_{m=N} * F_j)(\mathbf{x}) = \frac{1}{N} \sum_{j=1}^N \int_{-\infty}^{\infty} dy P_{m=N}(x_1, \dots, x_{j-1}, y, x_{j+1}, \dots, x_N) \frac{1}{\ell_{N-1}} \mathcal{R}\left(\frac{|x_j - y|}{\ell_{N-1}}\right), \quad (\text{S43})$$

where the symbol $*$ indicates a convolution. The interpretation of this expression is straightforward. At every reset event, all particles except one are brought back to the origin. As a result, the stationary state can be constructed by taking the stationary JPDF $P_{m=N}(\mathbf{x})$, corresponding to the fully simultaneous resetting, and replacing the coordinate of the particle that is not reset with a position drawn from its one-body stationary distribution $\frac{1}{\ell_{N-1}} \mathcal{R}\left(\frac{|x_j - y|}{\ell_{N-1}}\right)$. Since any of the N particles can play this role with equal probability, the final stationary distribution is obtained by averaging this construction over all possible choices of that particle.

S5. JPDF FOR $m = 1$

In the case $m = 1$, each time a reset event occurs only a single particle is reset, while the remaining $N - 1$ continue their diffusive motion unperturbed. As no two particles are ever reset simultaneously, the sole mechanism capable of generating correlations is absent, since there are no direct interactions between the particles. Consequently, the JPDF must factorize into a product of single-particle distributions. Because all particles play the same role in the system, each one-point marginal must coincide with the average particle density. The JPDF therefore takes the form

$$P_{m=1}(\mathbf{x}) = \prod_{i=1}^N \rho_N^1(x_i), \quad (\text{S44})$$

where $\rho_N^{m=1}(x)$ is the one-point marginal given in (S31). Explicitly,

$$P_{m=1}(\mathbf{x}) = \prod_{i=1}^N \frac{1}{2\ell_1} e^{-|x_i|/\ell_1}, \quad \ell_1 = \sqrt{\frac{ND}{r}}. \quad (\text{S45})$$

One may also take the FT of (S45) and check that it is solution of (S28).

S6. CORRELATORS: $\mathcal{C}_2(t)$ AND $a(t; m, N)$

As discussed in the main text, the global flip symmetry $x_i \rightarrow -x_i$ implies that the first non-trivial correlations of a pair of particles in the system are captured by the 2×2 correlation matrix \mathbf{C} , defined by

$$C_{ij}(t) = \langle x_i^2(t) x_j^2(t) \rangle - \langle x_i^2(t) \rangle \langle x_j^2(t) \rangle, \quad i, j \in \{1, 2\}. \quad (\text{S46})$$

Permutation symmetry among the particles immediately yields

$$C_{ii}(t) = \mathcal{C}_1(t) = \langle x_i^4(t) \rangle - \langle x_i^2(t) \rangle^2, \quad (\text{S47})$$

$$C_{ij}(t) = \mathcal{C}_2(t) = \langle x_i^2(t) x_j^2(t) \rangle - \langle x_i^2(t) \rangle \langle x_j^2(t) \rangle, \quad i \neq j. \quad (\text{S48})$$

We then introduce the normalized correlation coefficient

$$a(t; m, N) = \frac{\mathcal{C}_2(t)}{\mathcal{C}_1(t)}. \quad (\text{S49})$$

Equivalently, since \mathbf{C} is symmetric and therefore admits two real eigenvalues (which we denote by $\lambda_+(t) > \lambda_-(t)$), one finds

$$a(t; m, N) = \frac{\lambda_+(t) - \lambda_-(t)}{\lambda_+(t) + \lambda_-(t)}. \quad (\text{S50})$$

The coefficient $a(t; m, N)$ lies in the interval $[0, 1]$: it vanishes when x_i^2 and x_j^2 are uncorrelated, and reaches unity when they are perfectly correlated.

The quantities in (S47) and (S49) can be computed in two equivalent ways. A first approach consists of multiplying eq. (S22) by an arbitrary observable $f(\mathbf{x})$ and integrating over all configurations \mathbf{x} . This yields a differential equation for the expectation value $\langle f(\mathbf{x}) \rangle$, which can then be explicitly solved for observables such as $f(\mathbf{x}) = x_i^2 x_j^2$, x_i^2 , or x_i^4 . Alternatively, one can work directly in Fourier space. From (S25), with the same reasoning used to derive (S29) and (S30), one can derive the expressions for the full time-dependent solutions of the marginals $\tilde{P}_1(k, t)$ and $\tilde{P}_2(k_1, k_2, t)$. The results are:

$$\tilde{P}_m^1(k, t) = \frac{\tilde{r}}{\tilde{r} + Dk^2} + \frac{Dk^2}{Dk^2 + \tilde{r}} e^{-(Dk^2 + \tilde{r})t} \quad (\text{S51})$$

and

$$\tilde{P}_m^2(k_1, k_2, t) = e^{-\lambda_2 t} + \frac{\tilde{r}(2 - \beta)}{\lambda_2} (1 - e^{-\lambda_2 t}) + \tilde{r}(\beta - 1) \sum_{j=1}^2 \left\{ \frac{\tilde{r}}{\gamma(k_j)} \frac{1 - e^{-\lambda_2 t}}{\lambda_2} + \left(1 - \frac{\tilde{r}}{\gamma(k_j)} \right) \frac{e^{-\gamma(k_j)t} - e^{-\lambda_2 t}}{\lambda_2 - \gamma(k_j)} \right\} \quad (\text{S52})$$

with

$$\lambda_2 = D(k_1^2 + k_2^2) + \tilde{r}\beta, \quad \gamma(k) = Dk^2 + \tilde{r}.$$

By differentiating Eqs. (S51) and (S52) the desired moments can be obtained through the identities:

$$\langle x_i^2(t) \rangle = - \frac{\partial^2 \tilde{P}_1(k, t)}{\partial k^2} \Big|_{k=0}, \quad \langle x_i^4(t) \rangle = \frac{\partial^4 \tilde{P}_1(k, t)}{\partial k^4} \Big|_{k=0}, \quad \langle x_i^2 x_j^2(t) \rangle = \frac{\partial^2}{\partial k_1^2} \frac{\partial^2}{\partial k_2^2} \tilde{P}_2(k_1, k_2, t) \Big|_{k_1, k_2=0}. \quad (\text{S53})$$

It is then straightforward to get

$$\mathcal{C}_1(t) = \frac{4D^2}{\tilde{r}^2} f_1(\tilde{r}t), \quad f_1(z) = 5 - 4e^{-z} - 6ze^{-z} - e^{-2z}, \quad (\text{S54})$$

$$\mathcal{C}_2(t) = \frac{4D^2}{\tilde{r}^2} f_2(\tilde{r}t; \beta), \quad f_2(z; \beta) = 2 \left(\frac{1 - e^{-\beta z}}{\beta} - \frac{e^{-z} - e^{-\beta z}}{\beta - 1} \right) - 1 - e^{-2z} + 2e^{-z}, \quad (\text{S55})$$

$$a(t; m, N) = A(\tilde{r}t; \beta), \quad A(z; \beta) = \frac{f_2(z; \beta)}{f_1(z)}. \quad (\text{S56})$$

where $\tilde{r} = \frac{m}{N}r$ and $\beta = \frac{2N-m-1}{N-1}$. We recall here that $\beta \in [1, 2]$, where $\beta = 1$ corresponds to the classical case with $m = N$, while $\beta = 2$ corresponds to $m = 1$. The function $f_2(z; \beta)$ has a diverging factor when $\beta \rightarrow 1$ ($m \rightarrow N$), but setting $\beta = 1 + \epsilon$ and taking the limit $\epsilon \rightarrow 0$ recovers the known result for the fully synchronous case: $f_2(z; 1) = 1 - 2ze^{-z} - e^{-2z}$ [2]. The asymptotics of these three functions, when $\beta > 1$, are

$$f_1(z) \approx \begin{cases} 2z^2, & z \rightarrow 0, \\ 5 - 6ze^{-z}, & z \rightarrow \infty. \end{cases} \quad (\text{S57})$$

$$f_2(z; \beta) \approx \begin{cases} \frac{2-\beta}{3} z^3, & z \rightarrow 0, \\ \left(\frac{2}{\beta} - 1 \right) - 2 \frac{2-\beta}{\beta-1} e^{-z}, & z \rightarrow \infty. \end{cases} \quad (\text{S58})$$

$$A(z; \beta) \approx \begin{cases} \frac{2-\beta}{6}z, & z \rightarrow 0^+, \\ \frac{1}{5} \left(\frac{2}{\beta} - 1 \right) + \left[\frac{6(2-\beta)}{25\beta}z + \frac{2(3\beta^2 - 4\beta - 4)}{25\beta(\beta-1)} \right] e^{-z}, & z \rightarrow \infty, \beta > 1. \end{cases} \quad (\text{S59})$$

S6.1. Analysis of the maximum $z^*(\beta)$ of $A(z; \beta)$

From Fig. S1 and Eq. (S59) one sees that $A(z; \beta)$ must have a maximum at some finite value $z^*(\beta)$ for any $1 < \beta < 2$. However, a closed analytical expression for $z^*(\beta)$ is difficult to obtain. Nevertheless, we can make progress by considering the regime $\beta = 1 + \epsilon$ with $\epsilon = \frac{N-m}{N-1}$ and by searching for an expansion of $z^*(\epsilon)$ for $\epsilon \rightarrow 0$ (i.e. $m \rightarrow N$, with N large). A numerical analysis shows (see Fig. S1) that $z^*(\epsilon) \rightarrow \infty$ as $\epsilon \rightarrow 0$. Therefore, when analyzing the

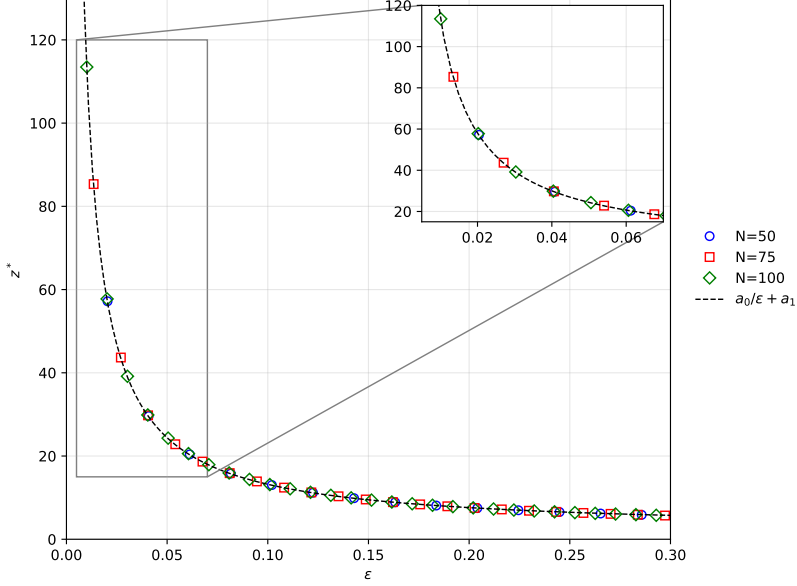


FIG. S1: Maximum $z^*(\beta = 1 + \epsilon)$ of $A(z; \beta)$ as a function of $\epsilon = \beta - 1 = \frac{N-m}{N-1}$. The dots correspond to numerical results, while the dashed line is the asymptotic expansion valid for small ϵ : $z^* = \frac{a_0}{\epsilon} + a_1$ with $a_0 = 1.1262\dots$ and $a_1 = 2$.

extremum condition $\partial_z A(z; \beta) = F(z, \beta) = 0$, we must take the joint limit $z \rightarrow \infty$, $\epsilon \rightarrow 0$ while keeping the product $z\epsilon$ finite. Expanding $F(z, 1 + \epsilon)$ in this double scaling limit yields, at leading order,

$$F(\beta = 1 + \epsilon, z) \approx \frac{2}{25} e^{-z\epsilon} e^{-z} \frac{e^{z\epsilon}(\epsilon-1)[-6(1+\epsilon) + 3\epsilon z + 1] - 5(1+\epsilon)}{\epsilon(1+\epsilon)}. \quad (\text{S60})$$

We now introduce the asymptotic ansatz

$$z^*(\epsilon) = \frac{a_0}{\epsilon} + a_1,$$

substitute it into (S60), expand for small ϵ , and set the coefficients of the various orders in ϵ to zero. This yields the coupled equations

$$e^{a_0}(5 - 3a_0) = 5, \quad e^{a_0}[(5 - 3a_0)(a_1 - 1) + 6 - 3a_1] = 5.$$

Solving them gives $a_0 = 1.1262\dots$ and $a_1 = 2$. Thus, for $\epsilon \rightarrow 0$ the position of the maximum diverges as

$$z^*(\epsilon) \simeq \frac{1.1262}{\epsilon} + 2. \quad (\text{S61})$$

This expansion is plotted in Fig.S1 together with the results of numerical locations of the maximum. For $\epsilon = 0$ exactly, the function $A(z; \beta = 1)$ is instead strictly monotonic in z .

We can also analyze the behavior of $z^*(\beta)$ in the limit $\beta \rightarrow 2^-$ (i.e. $N \rightarrow \infty$ and $m > 1$). In this regime, the amplitude of the scaling function $A(z; \beta)$ vanishes, as correlations disappear when particles are never reset together. Nevertheless, the position of the maximum remains finite:

$$z^*(\beta \rightarrow 2^-) \rightarrow \bar{z} = 2.6495 \dots \quad (\text{S62})$$

Thus, throughout the whole interval $1 < \beta < 2$, the decorrelation mechanism generated by batch resetting is characterized by a timescale which is always greater than \bar{z} . The function $z^*(\beta)$ interpolates between the finite limit \bar{z} at $\beta \rightarrow 2^-$ and the divergent behavior obtained as $\beta \rightarrow 1^+$. The result in (S62) can be derived by setting $\beta = 2 - \delta$ with $\delta = \frac{m-1}{N-1}$ in (S56), expanding to first order in δ , differentiating with respect to z , and imposing the extremum condition. This leads to the equation

$$6e^z z^2 + 13e^z z - 10e^{2z} z - 3e^{3z} z + 13e^z - 23e^{2z} + 11e^{3z} - 1 = 0, \quad (\text{S63})$$

whose numerical solution yields $\bar{z} = 2.6495 \dots$

S6.2. Stationary correlators

We have already obtained the full time dependence of the second-order correlations between a pair of particles, namely

$$\mathcal{C}_2(t) = \langle x_i^2(t) x_j^2(t) \rangle - \langle x_i^2(t) \rangle \langle x_j^2(t) \rangle, \quad i \neq j. \quad (\text{S64})$$

This function depends on the number of particles N and the number of reset particles m ; its explicit expression is given in (S55). For notational simplicity, we omit the explicit dependence on m and N in (S64). Taking the limit $t \rightarrow \infty$ limit in (S55) and using $\beta = \frac{2N-m-1}{N-1}$ we get the stationary correlator

$$\mathcal{C}_2^* = \mathcal{C}_2(t \rightarrow \infty) = \frac{4D^2}{r^2} V(m, N), \quad V(m, N) = \frac{N^2(m-1)}{m^2(2N-m-1)}. \quad (\text{S65})$$

It is interesting to study the extrema of the function $V(m, N)$. To this end, we first treat m as a continuous variable and analyze the stationary points obtained from the condition

$$\frac{dV(m, N)}{dm} = 0. \quad (\text{S66})$$

The solutions of this equation provide candidate extrema in the continuous variable m . Since m is restricted to integer values, the location of the maximum (or minimum) is then determined by evaluating $V(m, N)$ at the integer values closest to the stationary points, and by comparing these values with those at the boundaries $m = 1$ and $m = N$. Note that the latter satisfy $V(1, N) = 0$ and $V(N, N) = 1$ for all $N \geq 2$. Setting the derivative $\frac{dV(m, N)}{dm}$ equal to zero yields

$$N^2 m [2m^2 - 2m(N+1) + 4N - 2] = 0, \quad (\text{S67})$$

which must be analyzed for $N \geq 2$ and $1 \leq m \leq N$. Discarding the trivial solution $m = 0$, we are left with the quadratic equation

$$m^2 - m(N+1) + 2N - 1 = 0. \quad (\text{S68})$$

For $N > 5$, (S68) admits two real solutions

$$m_{\pm} = \frac{(N+1) \pm \sqrt{(N-1)(N-5)}}{2}. \quad (\text{S69})$$

The larger root m_+ corresponds to a local minimum, while the smaller root m_- corresponds to a maximum. Moreover, for $N \geq 6$ one finds $2 < m_- < 3$. Since m must be an integer, the maximum of $V(m, N)$ for $N \geq 6$ must occur at either $m = 2$ or $m = 3$. We therefore compare

$$V(2, N) = \frac{N^2}{4(2N-3)}, \quad V(3, N) = \frac{2N^2}{9(2N-4)}. \quad (\text{S70})$$

A direct comparison shows that $V(2, N) > V(3, N) > 1$ for all $N > 6$. Hence, for $N > 6$, the global maximum of $V(m, N)$ over the integers $m \in [1, N]$ is attained at $m = 2$.

For $N = 6$, instead, one finds $V(2, 6) = V(3, 6) = V(6, 6) = 1$, so that the maximum is not unique and it is attained for three distinct values of m .

For $N = 5$, the two solutions m_+ and m_- coincide and correspond to an inflection point. Thus, in this case, the function $V(m, 5)$ is monotonically increasing in the interval $m \in [1, 5]$, and its maximum is reached at the boundary $m = 5$.

Finally, for $N < 5$, (S68) has no real solutions, indicating the absence of local extrema in the open interval $m \in (1, N)$. The function $V(m, N)$ is therefore monotonic, and its maximum is again attained at the boundary $m = N$.

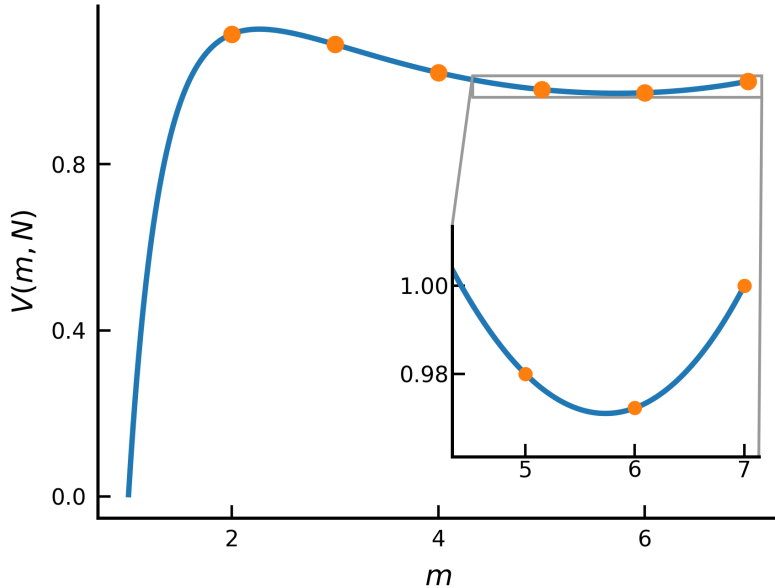


FIG. S2: Plot of the function $V(m, N = 7)$ given in (S65). The inset clearly shows the local minimum at $m = N - 1 = 6$.

As anticipated, the point m_+ corresponds to a local minimum of the function $V(m, N)$ when $N > 5$. Moreover, for $N > 5$ one has $N - 2 < m_+ < N - 1$. Since m must take integer values, the discrete minimum in the vicinity of m_+ must therefore occur either at $m = N - 2$ or $m = N - 1$. Evaluating $V(m, N)$ at these two values yields

$$V(N - 1, N) = \frac{N(N - 2)}{(N - 1)^2}, \quad V(N - 2, N) = \frac{N^2(N - 3)}{(N - 2)^2(N + 1)}. \quad (\text{S71})$$

A direct comparison shows that $V(N - 1, N) < V(N - 2, N) < 1$, which implies that, for all $N > 5$, the function $V(m, N)$ attains a local minimum at $m = N - 1$. It is also useful to rewrite

$$V(N - 1, N) = 1 - \frac{1}{(N - 1)^2}, \quad (\text{S72})$$

which makes it explicit that this minimum lies strictly below unity, while its deviation from 1 is small and it vanishes as $N \rightarrow \infty$.

This analysis shows that the function $V(m, N)$, which quantifies the strength of stationary correlations, undergoes a qualitative change when the number of particles N crosses the critical value $N_c = 6$. For $N < N_c$, $V(m, N)$ increases monotonically with m , whereas for $N > N_c$ it becomes non-monotonic. As a result, the global maximum shifts discontinuously from the boundary $m = N$ to the interior value $m = 2$ as N crosses N_c . In this regime, $V(m, N)$ also develops a shallow local minimum at $m = N - 1$, whose depth decreases with increasing N and vanishes in the limit $N \rightarrow \infty$. At the critical point $N = N_c$, the maximum is degenerate, and $V(m, N_c)$ attains the same maximal value 1 for $m = 2$, $m = 3$, and $m = N$.

It is also interesting to study the large N asymptotics of the function $V(m, N)$. It displays two distinct regimes, depending on how m scales with N :

(i) $m = \kappa N$ with $0 < \kappa \leq 1$. If a finite fraction κ of the particles is reset at each event, then

$$V(m, N) \xrightarrow[N \rightarrow \infty]{} \tilde{v}_1(\kappa) = \frac{1}{\kappa(2 - \kappa)}. \quad (\text{S73})$$

This limit is regular for any $0 < \kappa < 1$, while it becomes singular as $\kappa \rightarrow 0$:

$$\tilde{v}_1(\kappa) \sim \frac{1}{2\kappa}. \quad (\text{S74})$$

This limit is noteworthy because $\tilde{v}_1(\kappa)$ diverges as $\kappa = m/N \rightarrow 0$, while for the extreme case $m = 1$ (corresponding to $\kappa = 0$) the function V remains identically zero, i.e. $V(m = 1, N) = 0$, for all N .

(ii) $m = O(1)$ as $N \rightarrow \infty$. When the number of reset particles does not grow with N , the behavior changes qualitatively. In this regime,

$$V(m, N) \xrightarrow[N \rightarrow \infty]{} N \tilde{v}_2(m), \quad \tilde{v}_2(m) = \frac{m-1}{2m^2}, \quad (\text{S75})$$

which means that $V(m, N)$ grows linearly with the system size. Here it is also clear that the function $\tilde{v}_2(m)$ reaches a maximum at $m = 2$. For large m ,

$$\tilde{v}_2(m) \sim \frac{1}{2m} \quad (m \rightarrow \infty), \quad (\text{S76})$$

which, as expected, matches the small- κ limit of $\tilde{v}_1(\kappa)$.

S7. PHYSICAL INTERPRETATION OF THE MAXIMUM OF $A(z; \beta)$

In order to understand, from a physical perspective, why the function $a(z = \tilde{r}t; m, N) = A(z; \beta)$ has a maximum, we can write a differential equation governing the time evolution of the quantities: $v(t) = \langle x_i^2(t) \rangle$, $\mathcal{C}_2(t) = \langle x_i^2(t) x_j^2(t) \rangle$, $\mathcal{C}_1(t) = \langle x_i^4(t) \rangle$ and $a(t; m, N)$. To do so, we can multiply (S22) for x_i^2 or x_i^4 or $x_i^2 x_j^2$, and integrate over all possible configurations \mathbf{x} . The results read as follows:

$$\frac{dv(t)}{dt} = 2D - \tilde{r}v(t), \quad \tilde{r} = \frac{m}{N}r, \quad (\text{S77})$$

$$\frac{d\mathcal{C}_1(t)}{dt} = -\tilde{r}\mathcal{C}_1(t) + 8Dv(t) + \tilde{r}v(t)^2, \quad (\text{S78})$$

$$\frac{d\mathcal{C}_2(t)}{dt} = -\tilde{r}\beta\mathcal{C}_2(t) + (2 - \beta)\tilde{r}v^2(t), \quad \beta = \frac{2N - m - 1}{N - 1}, \quad (\text{S79})$$

These equations can be used to derive a differential equation for $a(t; m, N) = \mathcal{C}_2(t)/\mathcal{C}_1(t)$. For notational simplicity, in the following we write $a(t)$ instead of $a(t; m, N)$ whenever no confusion arises. Using Eqs. (S78) and (S79), we obtain

$$\frac{da(t)}{dt} = \frac{d}{dt} \frac{\mathcal{C}_2(t)}{\mathcal{C}_1(t)} = \frac{1}{\mathcal{C}_1(t)} \left[\frac{d\mathcal{C}_2(t)}{dt} - a(t) \frac{d\mathcal{C}_1(t)}{dt} \right] = -(\beta - 1)\tilde{r}a(t) + (2 - \beta)\tilde{r} \frac{v^2(t)}{\mathcal{C}_1(t)} - a(t) \frac{8Dv(t) + \tilde{r}v^2(t)}{\mathcal{C}_1(t)}. \quad (\text{S80})$$

We now need to solve (S77) and (S78) explicitly. The results read

$$v(t) = \frac{2D}{\tilde{r}}(1 - e^{-\tilde{r}t}), \quad \text{and} \quad \mathcal{C}_1(t) = \left(\frac{2D}{\tilde{r}} \right)^2 f_1(\tilde{r}t), \quad f_1(z) = 5 - 4e^{-z} - 6z e^{-z} - e^{-2z}. \quad (\text{S81})$$

We can now insert these expressions into (S80). Introducing the rescaled time $z = \tilde{r}t$, the differential equation for the scaling function $A(z; \beta) \equiv a(\tilde{r}t; m, N)$ reads

$$\frac{dA(z; \beta)}{dz} = - \left[(\beta - 1) + \omega(z) + \phi(z) \right] A(z; \beta) + (2 - \beta) \phi(z), \quad (\text{S82})$$

where

$$\omega(z) = \frac{4(1 - e^{-z})}{f_1(z)}, \quad \phi(z) = \frac{(1 - e^{-z})^2}{f_1(z)}. \quad (\text{S83})$$

These functions behave as

$$\phi(z) \approx \begin{cases} \frac{1}{2} - \frac{z}{4}, & z \rightarrow 0, \\ \frac{1}{5} + \frac{6}{25}(z-1)e^{-z}, & z \rightarrow \infty, \end{cases} \quad (\text{S84})$$

$$\omega(z) \approx \begin{cases} \frac{2}{z} + \frac{z}{6}, & z \rightarrow 0, \\ \frac{4}{5} + \left(\frac{24z-4}{25}\right)e^{-z}, & z \rightarrow \infty. \end{cases} \quad (\text{S85})$$

Equation (S82) shows that the evolution of $A(z; \beta)$ is governed by two distinct types of contributions: negative terms proportional to $A(z; \beta)$, which erase pre-existing correlations, and a source term, $(2 - \beta)\phi(z)$, which generates new correlations. The balance between these competing effects determines the overall correlation strength. Diffusion acts as a purely decorrelating mechanism, encoded in the term $\omega(z)A(z; \beta)$: during diffusive motion, particles evolve independently and any existing correlations are progressively washed out. Resetting also destroys correlations, because whenever a reset occurs the past trajectory of the reset particle is forgotten. This loss of memory is captured by the term $\phi(z)A(z; \beta)$, which is present even when all particles are reset simultaneously. However, resetting does not only erase correlations: it can also create them. When two particles are reset simultaneously, they are brought to the same position and correlations are reinjected into the system. This effect appears through the source term $(2 - \beta)\phi(z)$, showing that the same function $\phi(z)$ that controls the loss of correlations due to resetting also controls their reinjection, provided the reset is synchronous. The prefactor $2 - \beta$ reflects the probability that the two particles are reset simultaneously: indeed, the corresponding rate $\tilde{r}(2 - \beta) = r m(m-1)/[N(N-1)]$ is precisely the probability per unit time that two fixed particles are reset in the same event. An additional decorrelation mechanism arises only when $m \neq N$ ($\beta \neq 1$). In this case, a reset event may affect one particle but not the other, thereby destroying their mutual correlation without any possibility of reinjection. This process is encoded in the term $(\beta - 1)A(z; \beta)$, whose rate $\tilde{r}(\beta - 1) = r m(N-m)/[N(N-1)]$ is precisely the probability that only one of the two particles is reset. The competition between correlation injection by synchronous resetting and correlation loss due to diffusion and asynchronous resetting leads to the non-monotonic behavior of $A(z; \beta)$. When $m = N$, asynchronous resetting is absent, the term $\beta - 1$ vanishes, and no decorrelation phase is observed. Thus, the additional decorrelating phase observed in batch resetting for $m \neq N$ originates entirely from asynchronous resetting events.

S8. CONNECTED PAIR CORRELATION FUNCTION

We now consider the large N limit, where our system of N particles turns into a strongly correlated gas in the continuum. To probe the correlations in such systems, we need to go beyond the correlations at the individual particle levels and instead study the density-density correlation functions of the gas. This can be done by coarse-graining the system by first defining the empirical density (normalised to unity)

$$\hat{\rho}(x) = \frac{1}{N} \sum_{i=1}^N \delta(x - x_i). \quad (\text{S86})$$

Its average is indeed the coarse-grained density profile given by

$$\langle \hat{\rho}(x) \rangle = \frac{1}{N} \left\langle \sum_{i=1}^N \delta(x - x_i) \right\rangle, \quad (\text{S87})$$

where the average is taken over the JPDF. Note that $\langle \hat{\rho}(x) \rangle$ then coincides with the one-point marginal discussed in the main text and also in Section S2, denoted by $P_m^1(x)$. The connected pair correlation function is then defined as

$$G(x, y) = \langle \hat{\rho}(x) \hat{\rho}(y) \rangle - \langle \hat{\rho}(x) \rangle \langle \hat{\rho}(y) \rangle. \quad (\text{S88})$$

The function $G(x, y)$ can also be re-expressed in terms of the one- and two-point marginals as

$$G(x, y) = P_m^2(x, y) - P_m^1(x)P_m^1(y) + \frac{1}{N} [P_m^1(x)\delta(x - y) - P_m^2(x, y)]. \quad (\text{S89})$$

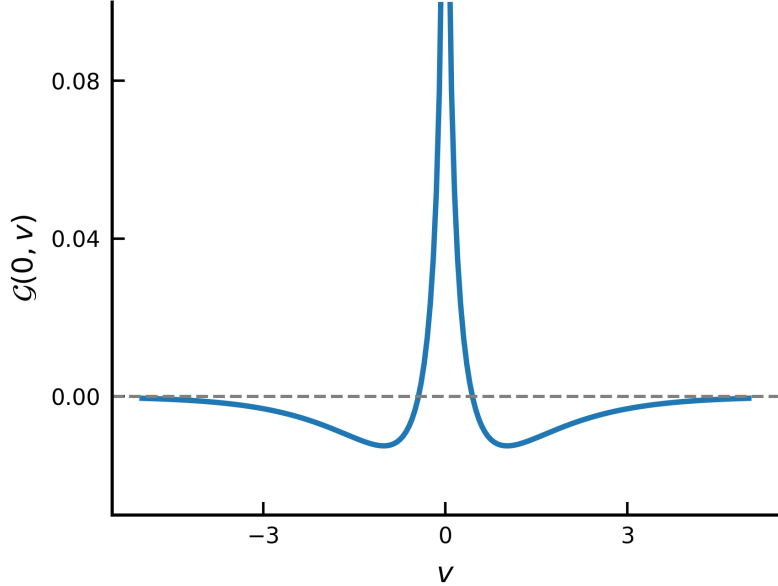


FIG. S3: Plot of $\mathcal{G}(u = 0, v)$ [given in (S93), setting $u = 0$] as a function of v .

It can then be computed explicitly by using the results from Eqs. (S31) and (S32). In the large N limit the last term in Eq. (S89) drops out, leading to

$$G(x, y) \approx P_m^2(x, y) - P_m^1(x)P_m^1(y) . \quad (\text{S90})$$

This pair correlation function also satisfies the sum rule

$$\int G(x, y) dy = 0 . \quad (\text{S91})$$

This simply follows from the definition in Eq. (S90). Indeed, when one integrates over y , the two-point marginal reduces to a one-point marginal and the integral of the one-point function is unity. The pair-correlation function $G(x, y)$ in Eq. (S90) can be expressed in the scaling form

$$G(x, y) = \frac{1}{\ell_m^2} \mathcal{G} \left(\frac{x}{\ell_m}, \frac{y}{\ell_m} \right) , \quad \text{where} \quad \ell_m^2 = \frac{D}{\tilde{r}} , \quad \text{with} \quad \tilde{r} = \frac{m}{N} r . \quad (\text{S92})$$

Using the results from Eqs. (S31) and (S32) the scaling function is given by

$$\mathcal{G}(u, v) = \mathcal{P}_\beta(u, v) - \mathcal{R}(u)\mathcal{R}(v) , \quad (\text{S93})$$

where $\mathcal{R}(u)$ and $\mathcal{P}_\beta(u, v)$ are defined respectively in (S31) and (S36). Note that this function $\mathcal{G}(u, v)$ depends on both coordinates u and v separately and not just on their difference, unlike in an isotropic and homogeneous gas. In Fig. S3, we show a plot of the function $\mathcal{G}(0, v)$. This function is symmetric around $v = 0$ and has the asymptotic behaviours

$$\mathcal{G}(u = 0, v) \approx \begin{cases} -\left(\frac{2-\beta}{2\pi} \ln\left(\frac{\sqrt{\beta}}{2}|v|\right)\right) , & v \rightarrow 0 , \\ -\frac{1-\sqrt{\beta-1}}{4} e^{-v} , & v \rightarrow \infty . \end{cases} \quad (\text{S94})$$

The logarithmic divergence at small v is a direct signature of simultaneous resetting and, as expected, its amplitude is controlled by the factor $(2 - \beta)$, which quantifies the probability of simultaneous reset events. Indeed, particles that are reset in the same event are reinjected at the same position, leading to an enhanced probability of finding particle pairs at vanishing separation and thus to a divergent short-distance behavior of the connected correlation function. For $u = 0$ and large v , the dominant contribution comes from asynchronous resetting events, in which one particle is reset to the origin ($u = 0$) while the other evolves freely and moves far away, resulting in an exponential decay of correlations controlled by $(\beta - 1)$. Note that due to the sum rule in Eq. (S91), we have $\int_0^\infty dv \mathcal{G}(0, v) = 0$, indicating that $\mathcal{G}(0, v)$ must change sign in some region of space, as seen in Fig. S3: thus the excess of probability at short distances induced by simultaneous resetting must be compensated by a depletion at larger separations.

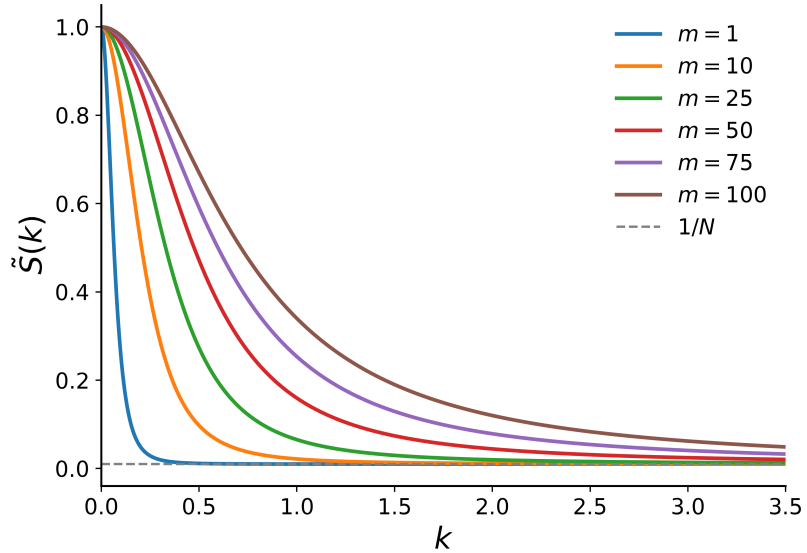


FIG. S4: Plot of $\tilde{S}(k)$ [given in (S99)] for $N = 100$ and different values of m .

S9. SPECTRAL FORM FACTOR

In this section, we study the spectral form factor of our system. We have defined the empirical density of particles as

$$\hat{\rho}(x) = \frac{1}{N} \sum_{i=1}^N \delta(x - x_i) \quad (\text{S95})$$

Its FT $\tilde{\rho}(k)$ reads

$$\tilde{\rho}(k) = \int_{-\infty}^{\infty} dx e^{ikx} \hat{\rho}(x) = \frac{1}{N} \sum_{i=1}^N e^{ikx_i} \quad (\text{S96})$$

We can then define the spectral form factor (*SFF*) as

$$SFF(k) = \frac{1}{N^2} \sum_{i,j} e^{ik(x_i - x_j)} = |\tilde{\rho}(k)|^2. \quad (\text{S97})$$

Since *SFF*(k) depends on the random variable x_i , we consider its average

$$\tilde{S}(k) = \langle SFF(k) \rangle = \frac{1}{N^2} \sum_{i,j} \langle e^{ik(x_i - x_j)} \rangle \quad (\text{S98})$$

This function captures the typical strength of the density fluctuations at wavelength $\frac{2\pi}{k}$. Eq. (S98) can be rewritten in terms of the FT of the 2-point marginal defined in (S30) as

$$\tilde{S}(k) = \frac{N-1}{N} \tilde{P}_m^2(k, -k) + \frac{1}{N} \quad (\text{S99})$$

where

$$\tilde{P}_m^2(k_1, k_2) = \frac{(2-\beta) + (\beta-1) \left[\tilde{P}_m^1(k_1) + \tilde{P}_m^1(k_2) \right]}{\beta + \ell_m^2(k_1^2 + k_2^2)}, \quad \text{with} \quad \tilde{P}_m^1(k) = \frac{1}{1 + \ell_m^2 k^2}, \quad (\text{S100})$$

$\beta = \frac{2N-m-1}{N-1}$, $\ell_m = \sqrt{\frac{D}{r}}$ and $\tilde{r} = \frac{m}{N}r$. This function behaves as

$$\tilde{S}(k) \simeq \begin{cases} 1 - 2\frac{N-1}{N} \ell_m^2 k^2 + O(k^4), & k \rightarrow 0, \\ \frac{1}{N} + \frac{1}{2} \frac{m-1}{N} \frac{1}{\ell_m^2} \frac{1}{k^2} + O\left(\frac{1}{k^4}\right), & k \rightarrow \infty. \end{cases} \quad (\text{S101})$$

To see the role played by inter-particle correlations, it is instructive to compare (S99) with the spectral form factor of a reference system in which the N particles are independent and identically distributed according to the same one-point marginal (S31). In this uncorrelated case, all nontrivial two-point information is lost, and the averaged spectral form factor reduces to

$$\tilde{S}_{\text{iid}}(k) = \frac{1}{N} + \frac{N-1}{N} \frac{1}{(1 + \ell_m^2 k^2)^2}. \quad (\text{S102})$$

The asymptotic behavior of $\tilde{S}_{\text{iid}}(k)$ is given by

$$\tilde{S}_{\text{iid}}(k) \simeq \begin{cases} 1 - \frac{2(N-1)}{N} \ell_m^2 k^2 + O(k^4), & k \rightarrow 0, \\ \frac{1}{N} + \frac{N-1}{N} \frac{1}{\ell_m^4 k^4} + O(k^{-6}), & k \rightarrow \infty. \end{cases} \quad (\text{S103})$$

Comparing the two cases, we observe that $\tilde{S}(k)$ and $\tilde{S}_{\text{iid}}(k)$ share the same small- k expansion, as expected since they are constructed from identical one-point marginals. However, their large- k behavior is qualitatively different. In particular, the slower k^{-2} decay of $\tilde{S}(k)$, as opposed to the k^{-4} decay of $\tilde{S}_{\text{iid}}(k)$, provides a clear spectral signature of the correlations induced by batch resetting.

S10. GENERALIZATION TO HIGHER DIMENSIONS d

In this section we extend our analysis to Brownian particles evolving in d spatial dimensions. We consider a system of N such particles, where the position of each one is described by a vector $\mathbf{x}_i = (x_{i,1}, \dots, x_{i,d}) \in \mathbb{R}^d$, where $i = 1, \dots, N$ labels the particle. We also define the vector $\mathbf{X} = (\mathbf{x}_1, \dots, \mathbf{x}_N) \in \mathbb{R}^{dN}$. In this setting, the Fokker–Planck equation in (S22) generalizes to

$$\partial_t P_m(\mathbf{X}, t) = D \sum_{i=1}^N \nabla_{\mathbf{x}_i}^2 P_m(\mathbf{X}, t) - r P_m(\mathbf{X}, t) + \frac{r}{\binom{N}{m}} \sum_{S_m} \left(\prod_{i \in S_m} \delta^{(d)}(\mathbf{x}_i) \right) P_m^{(N-m)}(\mathbf{X}_{S_m^c}, t), \quad (\text{S104})$$

Here we have defined $\nabla_{\mathbf{x}_i}^2 = \sum_{\alpha=1}^d \frac{\partial^2}{\partial x_{i,\alpha}^2}$ and $\delta^{(d)}(\mathbf{x}_i) = \prod_{\alpha=1}^d \delta(x_{i,\alpha})$. As in the $d = 1$ case studied above, the set S_m is a subset $S_m \subseteq \{1, \dots, N\}$ of size $|S_m| = m$, which is selected uniformly at random at each reset event. The set S_m^c is the complementary set, i.e. $S_m^c = \{1, \dots, N\} \setminus S_m$. The vector $\mathbf{X}_{S_m^c}$ is obtained from the vector \mathbf{X} by marginalizing over the vectors \mathbf{x}_i for all $i \in S_m$. We have also defined the JPDF $P_m(\mathbf{x}_1, \dots, \mathbf{x}_N, t) = P_m(\mathbf{X}, t)$, which now is a function of $Nd + 1$ variables. The function $P_m^{(N-m)}$ indicates the $(N-m)$ -particles marginal, i.e. the JPDF marginalized over all the d components of m different particles, namely

$$P_m^{(N-m)}(\mathbf{X}_{S_m^c}, t) = \iint d\mathbf{X}_{S_m} P_m(\mathbf{X}, t), \quad (\text{S105})$$

where $d\mathbf{X}_{S_m} = \prod_{i \in S_m} d\mathbf{x}_i = \prod_{i \in S_m} \prod_{j=1}^d dx_{i,j}$. Taking the FT of (S104), defined as

$$\tilde{P}_m(\mathbf{k}_1, \dots, \mathbf{k}_N, t) = \iint \prod_{i=1}^N d^d \mathbf{x}_i \exp\left(i \sum_{i=1}^N \mathbf{k}_i \cdot \mathbf{x}_i\right) P_m(\mathbf{x}_1, \dots, \mathbf{x}_N, t), \quad (\text{S106})$$

we obtain

$$\partial_t \tilde{P}_m(\mathbf{K}, t) = - \left(D \sum_{i=1}^N |\mathbf{k}_i|^2 + r \right) \tilde{P}_m(\mathbf{K}, t) + \frac{r}{\binom{N}{m}} \sum_{S_m} \tilde{P}_m^{N-m}(\mathbf{K}_{S_m^c}, t), \quad (\text{S107})$$

where we have set $\mathbf{K} = (\mathbf{k}_1, \dots, \mathbf{k}_N) \in \mathbb{R}^{Nd}$ and $P_m(\mathbf{k}_1, \dots, \mathbf{k}_N, t) = P_m(\mathbf{K}, t)$. The vector $\mathbf{K}_{S_m^c}$ is obtained from \mathbf{K} by setting the vector $\mathbf{k}_i = \mathbf{0}$ for all $i \in S_m$ and \tilde{P}_m^{N-m} is the FT of the $(N-m)$ -particles marginal.

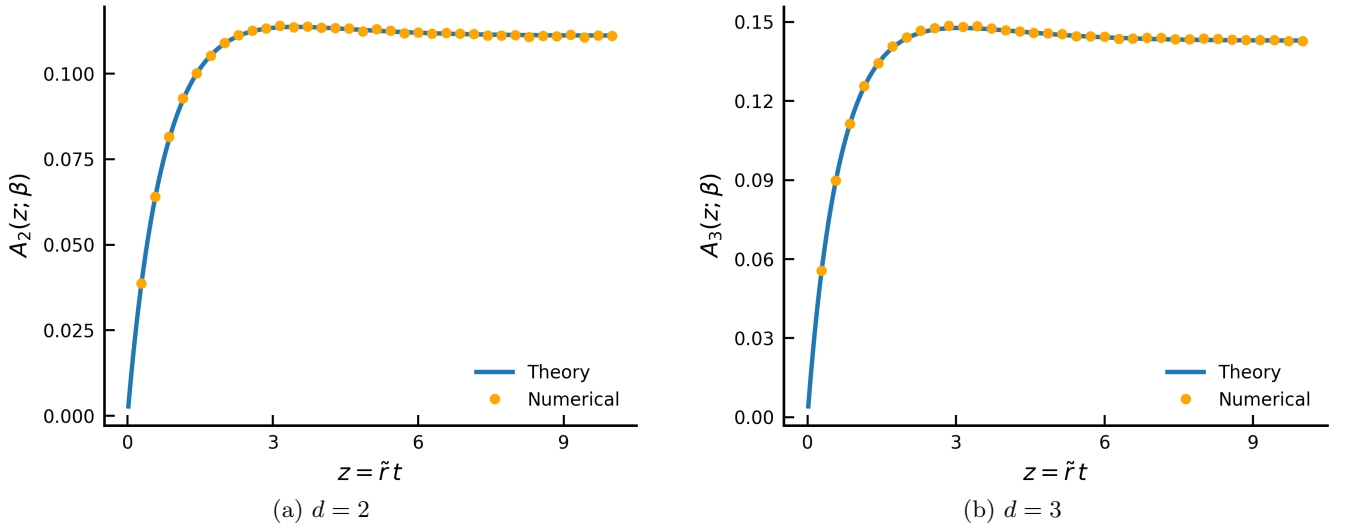


FIG. S5: Comparison between the results of numerical simulations (orange dots) and the theoretical prediction for the function $A_d(z; \beta)$ given in (S114). The left panel corresponds to $d = 2$, while the right panel corresponds to $d = 3$.

S10.1. Correlations

The correlators introduced in the Letter and defined in (S46) extend straightforwardly to particles evolving in d spatial dimensions. We define

$$\mathcal{C}_{1,d}(t) = \langle |\mathbf{x}_i|^4(t) \rangle - \langle |\mathbf{x}_i|^2(t) \rangle^2, \quad (\text{S108})$$

while, for $i \neq j$,

$$\mathcal{C}_{2,d}(t) = \langle |\mathbf{x}_i|^2(t) |\mathbf{x}_j|^2(t) \rangle - \langle |\mathbf{x}_i|^2(t) \rangle \langle |\mathbf{x}_j|^2(t) \rangle. \quad (\text{S109})$$

The normalized correlator then reads

$$a_d(t; m, N) = \frac{\mathcal{C}_{2,d}(t)}{\mathcal{C}_{1,d}(t)}. \quad (\text{S110})$$

Repeating the calculation of Sec. S6, starting from the Fokker–Planck equations (S104) or (S107), we obtain

$$\mathcal{C}_{1,d}(t) = \frac{4D^2}{\tilde{r}^2} f_{1,d}(\tilde{r}t), \quad \text{where} \quad f_{1,d}(z) = d(d+4) - 2d(2+z(2+d)) e^{-z} - d^2 e^{-2z}, \quad (\text{S111})$$

and

$$\mathcal{C}_{2,d}(t) = \frac{4D^2}{\tilde{r}^2} f_{2,d}(\tilde{r}t; \beta), \quad \text{where} \quad f_{2,d}(z; \beta) = d^2 \left[2 \left(\frac{1 - e^{-\beta z}}{\beta} - \frac{e^{-z} - e^{-\beta z}}{\beta - 1} \right) - 1 - e^{-2z} + 2e^{-z} \right]. \quad (\text{S112})$$

We recall that $z = \tilde{r}t$ with $\tilde{r} = \frac{m}{N}r$ and $\beta = \frac{2N-m-1}{N-1}$. We clearly see from (S112) that the function $\mathcal{C}_{2,d}(t)$ scales trivially with d , i.e. $\mathcal{C}_{2,d}(t) = d^2 \mathcal{C}_{2,1}(t)$, while $\mathcal{C}_{1,d}(t)$ acquires a nontrivial d -dependence. By setting $d = 1$ in (S111) and (S112) we recover the results in (S54) and (S55).

Taking the long-time limit of Eq. (S112), we obtain the stationary correlator $\mathcal{C}_{2,d}^* = \mathcal{C}_{2,d}(t \rightarrow \infty)$, namely

$$\mathcal{C}_{2,d}^* = d^2 \frac{4D^2}{r^2} V(m, N), \quad V(m, N) = \frac{N^2(m-1)}{m^2(2N-m-1)}. \quad (\text{S113})$$

The function $V(m, N)$ coincides with the one-dimensional result [Eq. (S65)], as it is independent of d . As a consequence, the critical particle number $N_c = 6$ remains unchanged in all dimensions and all the remarks made for $d = 1$ in Sec. S6 remain valid in general.

We can also obtain the scaling function $A_d(z; \beta) = a_d(\tilde{r}t; m, N)$, which reads

$$A_d(z; m, N) = \frac{f_{2,d}(z; \beta)}{f_{1,d}(z)} = \frac{d \left[2 \left(\frac{1-e^{-\beta z}}{\beta} - \frac{e^{-z}-e^{-\beta z}}{\beta-1} \right) - 1 - e^{-2z} + 2e^{-z} \right]}{(d+4) - 2(2+z(2+d))e^{-z} - de^{-2z}}. \quad (\text{S114})$$

By setting $d = 1$ in the above expression, we recover (S56). From this expression, we find that in any dimension d the function $A_d(z; \beta)$ displays a maximum at a finite $z^*(\beta)$, for any $1 < \beta < 2$. In Fig. S5 we show (S114) for $d = 2$ and $d = 3$ together with the results of numerical simulations.

Repeating the same analysis done in Sec. S6 for $d = 1$, we can obtain the value of the maximum analytically in the two limits $\beta \rightarrow 1^+$ and $\beta \rightarrow 2^-$.

(i) When $\beta \rightarrow 1^+$, the location of the maximum $z^*(\beta)$ behaves as $z^*(\beta) \simeq \frac{a_0(d)}{\beta-1} + a_1$, where $a_0(d)$ and a_1 are the solutions of the system

$$(4 - 2a_0 + d - a_0 d) e^{a_0} = 4 + d \quad (\text{S115})$$

$$(2a_0 + 2a_1 - 2a_0 a_1 + d + a_0 d - a_0 a_1 d) e^{a_0} = 4 + d. \quad (\text{S116})$$

It turns out that $a_1 = 2$ exactly and for all dimensions d . In contrast, $a_0 = a_0(d)$ depends on d , and it is the solution of (S115). Defining $c = \frac{d+4}{d+2} > 1$, (S115) can be rewritten as

$$(c - a_0) e^{a_0} = c. \quad (\text{S117})$$

We can now express $a_0(d)$ as

$$a_0 = c + W(-ce^{-c}), \quad (\text{S118})$$

where $W(z)$ is the Lambert W function, defined as the solution of $z = W(z)e^{W(z)}$. In the large d limit we can set $c = \frac{d+4}{d+2} = 1 + \epsilon$ with $\epsilon = \frac{2}{d+2}$. We can then use the expansion (see [3])

$$W\left(-\frac{1}{e} + \delta\right) \approx -1 + \sqrt{2e\delta} \quad (\text{S119})$$

valid for small δ , where $\delta = \frac{\epsilon^2}{2e}$ in our case. This gives us $W(c) \approx -1 + \epsilon$ and so

$$a_0(d) \simeq 2\epsilon \simeq \frac{4}{d}. \quad (\text{S120})$$

in the limit of large d .

(ii) In the opposite limit ($\beta \rightarrow 2^-$), we find that $z^*(\beta)$ converges to a finite value $z^*(\beta \rightarrow 2^-) = \bar{z}(d)$ for any finite d ,

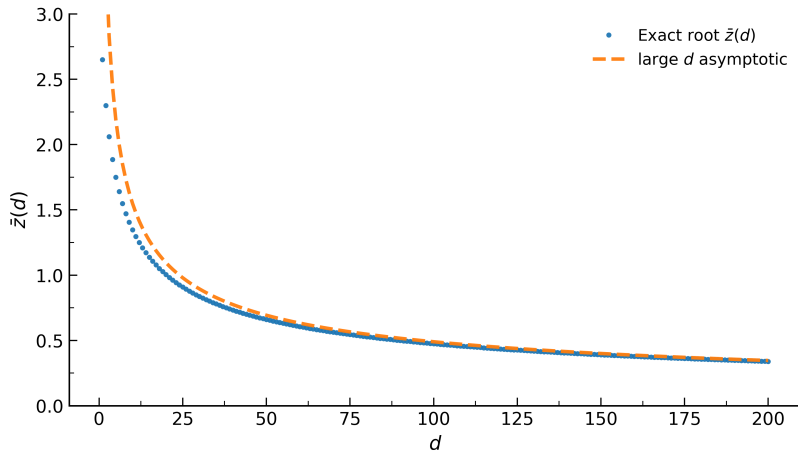


FIG. S6: The blue dots represent the numerical results for $\bar{z}(d)$, obtained by solving (S121). The orange dashed line shows the large- d asymptotic approximation of $\bar{z}(d)$, as given by (S124).

where $\bar{z}(d)$ is the solution of the equation

$$e^{3z}(8 + 3d - (2 + d)z) - e^{2z}(16 + 7d + 2(4 + d)z) + e^z(8 + 2z(5 + 2z) + d(5 + z(3 + 2z))) = d. \quad (\text{S121})$$

In Fig. S6 we show the numerical solution of (S121) as a function of d . From the numerical analysis, we observe that the solution $\bar{z}(d)$ decreases as d increases, suggesting that $\bar{z}(d) \rightarrow 0$ in the limit $d \rightarrow \infty$. We can therefore expand (S121) for small z , obtaining

$$\frac{2}{3}z^4 + z^5 + \left(\frac{34}{45} - \frac{d}{36}\right)z^6 + O(z^7) = 0. \quad (\text{S122})$$

We assume a power-law scaling of the form $\bar{z}(d) \sim d^{-\alpha}$ for large d . Substituting this ansatz into (S122), the different contributions scale as $z^4 \sim d^{-4\alpha}$, $z^5 \sim d^{-5\alpha}$, and $dz^6 \sim d^{1-6\alpha}$. A nontrivial solution requires a dominant balance between two leading terms. Balancing the $O(z^4)$ and $O(dz^6)$ contributions fixes the exponent to be $\alpha = \frac{1}{2}$. With this choice, all remaining terms are subdominant in the limit $d \rightarrow \infty$, confirming the self-consistency of the scaling ansatz. We therefore set

$$\bar{z}(d) \simeq \frac{c_0}{\sqrt{d}}, \quad d \gg 1. \quad (\text{S123})$$

Substituting this expression back into (S122) and retaining only the leading-order terms yields an algebraic equation for the prefactor c_0 , whose nontrivial solution is $c_0 = 2\sqrt{6}$. We thus obtain the asymptotic behavior

$$\bar{z}(d) \simeq \frac{2\sqrt{6}}{\sqrt{d}}, \quad d \rightarrow \infty. \quad (\text{S124})$$

This asymptotic prediction, together with the numerical determination of $\bar{z}(d)$, is shown in Fig. S6.

[1] M. Biroli, H. Larralde, S. N. Majumdar, and G. Schehr, Phys. Rev. Lett. **130**, 227101 (2023).
[2] G. de Mauro, M. Biroli, S. N. Majumdar, and G. Schehr, Phys. Rev. E **113**, 014120 (2026).
[3] R. M. Corless, G. H. Gonnet, D. E. G. Hare, D. J. Jeffrey, and D. E. Knuth, Adv. Comput. Math. **5**, 329–359 (1996).